

SOLVING HIGH-DIMENSIONAL HAMILTON-JACOBI-BELLMAN EQUATIONS WITH FUNCTIONAL HIERARCHICAL TENSOR

XUN TANG*, NAN SHENG†, AND LEXING YING‡

Abstract. This work proposes a novel numerical scheme for solving the high-dimensional Hamilton-Jacobi-Bellman equation with a functional hierarchical tensor ansatz. We consider the setting of stochastic control, whereby one applies control to a particle under Brownian motion. In particular, the existence of diffusion presents a new challenge to conventional tensor network methods for deterministic optimal control. To overcome the difficulty, we use a general regression-based formulation where the loss term is the Bellman consistency error combined with a Sobolev-type penalization term. We propose two novel sketching-based subroutines for obtaining the tensor-network approximation to the action-value functions and the value functions, which greatly accelerate the convergence for the subsequent regression phase. We apply the proposed approach successfully to two challenging control problems with Ginzburg-Landau potential in 1D and 2D with 64 variables.

Key words. High-dimensional Hamilton-Jacobi-Bellman equation; Semigroup method; Functional tensor network; Hierarchical tensor network; Curse of dimensionality.

MSC codes. 65M99, 15A69, 65F99

1. Introduction. This paper focuses on solving the Hamilton-Jacobi-Bellman (HJB) equation:

$$(1.1) \quad \begin{cases} \partial_t v(x, t) + \sup_{a \in A} [b(x, a) \cdot \nabla v(x, t) + f(x, a)] + \frac{1}{\beta} \Delta v(x, t) = 0, & x \in \mathcal{X} \subset \mathbb{R}^d, t \in [0, T], \\ v(y, T) = h(y), & y \in \mathcal{X} \subset \mathbb{R}^d, \end{cases}$$

where $A \subset \mathbb{R}^m$ is the set of controls, β is the inverse temperature controlling the diffusion coefficient, and the functions b, f, h respectively encode the drift, running cost, and terminal cost of a stochastic control problem.

The HJB equation solution gives the optimal value function of its associated stochastic control problem. Let $(\Omega, \mathcal{F}, \{\mathcal{F}_t\}_{t \in [0, T]}, \mathbf{P})$ be a filtered probability space. The PDE in Equation (1.1) models a stochastic control problem under the SDE dynamics:

$$(1.2) \quad dX_t = b(X_t, a_t)dt + \sqrt{2\beta^{-1}}dB_t,$$

where B_t is an \mathcal{F}_t -standard Brownian motion, and $a_t \in A$ is an \mathcal{F}_t -adapted control. The cost functional J is defined by the following equation:

$$(1.3) \quad J(t, y; (a_s)_{s \in [t, T]}) = \mathbb{E} \left[\int_t^T f(X_s, a_s)ds + h(X_T) \mid X_t = y \right],$$

where the expectation is taken with respect to the trajectory of the Brownian motion. The solution v to Equation (1.1) can be represented as $v(x, t) = \inf_{(a_s)_{s \in [t, T]}} \mathbb{E} [J(t, x, (a_s)_{s \in [t, T]})]$. In other words, v is the expected cumulative cost function under the optimal policy. We refer the readers to [51] for details.

The stochastic control problem is a prevalent task in science and engineering with a wide range of applications. In this work, we focus on the general setting in which the drift term b is non-linear and the spatial variable x is in a high-dimensional space. In particular, this setting is challenging and precludes the application of traditional methods such as stochastic linear quadratic control [4], finite volume methods [48], or Galerkin methods [3, 2].

*First author. Institute for Computational and Mathematical Engineering, Stanford, CA 94305, USA. (xuntang@stanford.edu).

†Institute for Computational and Mathematical Engineering, Stanford, CA 94305, USA. (nansheng@stanford.edu).

‡Department of Mathematics and Institute for Computational and Mathematical Engineering, Stanford, CA 94305, USA. (lexing@stanford.edu)

Funding: This work is partially supported by NSF grants DMS-2011699 and DMS-2208163.

In this work, we propose to use the parametric class of functional hierarchical tensor (FHT) [16, 17], which has been recently applied to solving the Fokker-Planck equation [45] and Kolmogorov backward equations [44]. This parametric class of functions is suitable for reduced-order modeling under a hierarchical low-rank structure. In general, FHT has a good approximation guarantee under sufficient regularity characterized by a Sobolev-type norm [39]. This work employs the strategies used in deep reinforcement learning [43] and adapts them to function classes based on tensor networks. As the optimization subroutines differ drastically from neural network approaches, one of the main contributions of this work is the development of a full workflow for stochastic optimal control under a tensor network ansatz.

Moreover, the use of the FHT function class is motivated by its applicability to model stochastic dynamics on function spaces, whereby the high-dimensional control problem comes from discretizing an infinite-dimensional Markov decision process. To give a motivating example, we consider the task of stabilizing a 2D field undergoing the gradient flow of a Ginzburg-Landau energy functional, a model widely used in the study of phase transitions and superconductivity. In the 2D G-L model, a “particle” takes the form of a field $x(z): [0, 1]^2 \rightarrow \mathbb{R}$. The Ginzburg-Landau potential is a functional $V(x)$ defined as follows:

$$(1.4) \quad V(x) = \frac{\lambda}{2} \int_{[0,1]^2} |\nabla_z x(z)|^2 dz + \frac{\mu}{4} \int_{[0,1]^2} |1 - x(z)^2|^2 dz,$$

where λ, μ are parameters balancing the relative importance of the first and second term in Equation (1.4), which respectively represents the gradient energy and the double-well potential. One can apply a coarse control $a \in \mathbb{R}$ with control direction $\omega: [0, 1]^2 \rightarrow \mathbb{R}$, and b admits the form

$$(1.5) \quad b(x, a) = -\nabla V(x) + a\omega.$$

Intuitively, the drift is in the direction of the gradient flow based on the Ginzburg-Landau functional, and the control applies a one-dimensional perturbation in the direction of ω , allowing for targeted influence on the system’s evolution.

Under discretization, one decomposes the unit square $[0, 1]^2$ into a grid of $d = m^2$ points $\{(ih, jh)\}$, for $h = \frac{1}{m+1}$ and $1 \leq i, j \leq m$. The discretized field is the d -dimensional vector $x = (x_{(i,j)})_{1 \leq i, j \leq m}$, where $x_{(i,j)} = x(ih, jh)$. The associated discretized potential energy is defined as

$$(1.6) \quad V(x) = V(x_{(1,1)}, \dots, x_{(m,m)}) := \left[\frac{\lambda}{2} \sum_{w \sim w'} \left(\frac{x_w - x_{w'}}{h} \right)^2 + \frac{\mu}{4} \sum_w (1 - x_w^2)^2 \right] h^2,$$

where w and w' are Cartesian grid points and $w \sim w'$ if and only if they are adjacent. Similarly, the control direction is discretized to the d -dimensional vector $\omega = (\omega_{(i,j)})_{1 \leq i, j \leq m}$, and the drift term is again described by Equation (1.5).

1.1. Related work.

Traditional methods in stochastic control. Various classical methods have been developed to solve stochastic control problems. Examples include the finite volume method [38, 47], the Galerkin method [3, 2], and the monotone approximation method [12]. For a detailed summary, we refer the readers to [37] and reference therein. While these methods provide accurate numerical solutions, they cannot be applied to high-dimensional HJB equations due to the curse of dimensionality.

Neural network methods. Great efforts have been made to solve high-dimensional HJB equations and related stochastic control problems using deep neural networks due to their effectiveness in high dimensions. One main approach is the deep backward stochastic differential equations (BSDE), where the BSDE formulation of HJB-type equations is parametrized and solved by deep neural networks [9, 19, 31, 36, 52]. Another approach is the physics-informed neural network [23, 26]. Other notable neural network approaches to tackle HJB equations include [18, 29, 28, 6]. While neural networks have been proven successful, algorithmic improvements might be difficult in general.

Tensor network methods. Tensor network methods provide reduced-order parameterizations for high-dimensional functions and have seen great applicability in scientific computing. Several tensor-network-related approaches have appeared in the literature to solve HJB or related optimal control problems. Examples include the canonical polyadic decomposition [22, 24, 5], the tensor train decomposition [40, 8, 7, 11, 14, 42, 27, 10, 13, 33, 34]. In this work, we adopt the functional hierarchical tensor for optimal control problems. In contrast to most existing work where the problem is deterministic, this work focuses on addressing numerical challenges in a setting where control is applied to a particle under Brownian motion. In particular, the existence of diffusion precludes the common strategy of approximating the expected cost function through black-box interpolation, such as the approach taken in [8, 40]. Specifically, we choose the functional hierarchical tensor ansatz because it is well suited for representing value functions when the state variable corresponds to a discretized 2D field.

Reinforcement learning. Reinforcement learning (RL) has attracted significant attention for its great success in the past decade [43]. The methodological development of RL techniques has laid a solid foundation for solving optimal control problems. Notable RL methods include Q-learning [50, 46] and the actor-critic method [25, 15]. Importantly, these methods have been extended to solving stochastic optimal control problems under function approximation, examples of which can be found in [1, 49, 52, 20]. The empirical success of RL methods is partly based on solving the regression problem over the Bellman consistency error, and our work uses a similar loss function over functional tensor network architecture.

1.2. Contents and notations. We outline the structure of the remainder of the manuscript. Section 2 goes through the algorithm for solving the HJB equation with the functional hierarchical tensor. Section 3 introduces the functional hierarchical tensor structures used in this work. Section 4 details the optimization procedure used in the main workflow. Section 5 presents the numerical experiments and associated implementation details.

For notational compactness, we introduce several shorthand notations for simple derivations. For $n \in \mathbb{N}$, let $[n] := \{1, \dots, n\}$. For an index set $S \subset [d]$, we let x_S stand for the subvector with entries from index set S . We use \bar{S} to denote the set-theoretic complement of S , i.e. $\bar{S} = [d] - S$.

2. Main formulation.

Temporal discretization of the HJB equation. To approximately solve the HJB equation in Equation (1.1), we propose to use a temporal discretization scheme whereby one selects time-steps $0 = t_0 < t_1 < \dots < t_K = T$ and restricts the control $(a_s)_{s \in [0, T]}$ to be locally constant on the region $s \in [t_k, t_{k+1}]$. Moreover, this work uses the natural choice of uniform grid spacing with $t_k = \frac{k}{K}T$. Under this discretization, the value function $v(x, t)$ admits the interpretation of the optimal expected cumulative cost under locally constant policies for time $s \in (t, T]$. Below $v(x, t_k)$ is often denoted as $v_k(x)$.

Q function. Under the proposed discretization scheme, the central object used in our formulation is the *action-value function*. We denote the action-value function for time $t = t_k$ as Q_k , defined as follows:

$$(2.1) \quad Q_k(x, a) = \mathbb{E} \left[\int_{s=t_k}^{t_{k+1}} f(X_s, a) ds + v(X_{t_{k+1}}, t_{k+1}) \mid (X_{t_k} = x) \wedge (\forall s \in [t_k, t_{k+1}], a_s = a) \right].$$

For the rest of this section, we explain the systematic procedure of using the Q_k function to obtain the value function v . Subsequently, we specify the structure of Q_k and give an overview of how to obtain Q_k .

Obtain v through backward time-stepping. With temporal discretization, the goal of solving Equation (1.1) is relaxed to finding the minimal expected cumulative cost function under locally constant controls. The proposed discretization scheme leads to a finite-horizon stochastic control problem with horizon K . This work treats the stochastic control problem with the standard backward time-stepping strategy. For $k = 0, \dots, K-1$, assume that $v(\cdot, t)$ has been solved for $t \in \{t_{k+1}, \dots, t_K = T\}$, and then the stochastic control problem at $t = t_k$ can be solved with access to Q_k defined by Equation (2.1). Specifically, one can form the optimal control at $t = t_k$ and state x by taking $a = \arg \min_{\hat{a} \in A} Q_k(x, \hat{a})$, and likewise, one can calculate the value function

at time $t = t_k$ from $v_k(x) = v(x, t_k) = \min_{\hat{a} \in A} Q_k(x, \hat{a})$. Subsequently, one obtains Q_{k-1} for the $t = t_{k-1}$, followed by solving v_{k-1} from Q_{k-1} . Overall, one can continue the backward time-stepping strategy until $t = t_0$ has been solved.

Obtain Q function through v. To obtain the action-value functions for each $t = t_k$, we propose to use the common Q -learning approach, for which we give a short introduction. One starts from selecting a collection of sampled state-action pairs $\{x^{(i)}, a^{(i)}\}_{i=1}^N$. For each state-action pair (x, a) , one evolves the SDE dynamics in Equation (1.2) with a fixed control a for a duration of $t_{k+1} - t_k = T/K$. After collecting the terminal state x' and the accumulated cost r for each state-action pair, one has the full collection of samples $\{x^{(i)}, a^{(i)}, (x')^{(i)}, r^{(i)}\}_{i=1}^N$. Then, the Q -learning procedure for Q_k is obtained with a regression task over the Bellman consistency error:

$$(2.2) \quad L(Q) = \frac{1}{N} \sum_{i=1}^N \left\| Q(x^{(i)}, a^{(i)}) - v_{k+1}((x')^{(i)}) - r^{(i)} \right\|_2^2,$$

and $v_k = v(\cdot, t_k)$ can be obtained from Q_k .

Function class of Q and v. In this work, we propose to represent the action-value functions $\{Q_k\}_{k=0}^{K-1}$ and value functions $\{v_k\}_{k=0}^{K-1}$ through the functional hierarchical tensor ansatz. As the stochastic optimal control problem comes from the discretization of function spaces, the function space discretization leads to a lattice structure, which makes the FHT ansatz an attractive candidate for functional approximation. We defer the details of this ansatz to Section 3.

Obtain continuous-in-time v. After the series of K control problems have been solved following backward propagation, one obtains the collection of action-value functions $\{Q_k\}_{k=0}^{K-1}$ and value functions $\{v_k := v(\cdot, t_k)\}_{k=0}^{K-1}$. To obtain the continuous-in-time solution for $v(\cdot, t)$ at non-grid points t , one first finds the index k for which $t \in [t_k, t_{k+1})$. Then, one can solve for the action-value function at time t following the definition in Equation (2.1) with t in place of t_k , and one then obtains $v(\cdot, t)$ by taking minimization over the action-value function. A more efficient alternative is to directly take the linear interpolation between v_k and v_{k+1} .

Summary of workflow. We summarize the workflow here:

1. Select K time steps $0 = t_0 < t_1 < \dots < t_K = T$ with $t_k = \frac{k}{K}T$.
2. Run N independent stochastic simulations on the stochastic dynamic equation Equation (1.2) on state-action pairs $\{x^{(i)}, a^{(i)}\}_{i=1}^N$ to time $\frac{T}{K}$.
3. Collect the associated terminal condition and the accumulated cost as $\{(x')^{(i)}, r^{(i)}\}_{i=1}^N$.
4. Starting at $k = K-1$, obtain an FHT approximation of Q_k by regression over the Bellman consistency error in Equation (2.2) with the collected samples $\{x^{(i)}, a^{(i)}, (x')^{(i)}, r^{(i)}\}_{i=1}^N$ and the previous time-step value function v_{k+1} . Then, use Q_k to obtain v_k . Iterate until one obtains Q_0, v_0 .
5. For any (x, t) , output the continuous-in-time solution either through computing the action-value function at time t or through linear interpolation.

3. Functional hierarchical tensor architecture. The defining feature of this work is the functional approximation with the functional hierarchical tensor (FHT) architecture, and we give a short introduction of this ansatz following the more detailed exposition in [45]. As is seen in Section 2, the FHT ansatz is used in the representation of three functions: (1) the value function $v: \mathbb{R}^d \rightarrow \mathbb{R}$ which maps state to the expected cumulative cost, (2) the action-value function $Q: \mathbb{R}^{d+m} \rightarrow \mathbb{R}$, which maps a state-action pair to the expected cumulative cost. Additionally, we consider (3) the Markov operator $P: \mathbb{R}^{d+d+m} \rightarrow \mathbb{R}$, which models the probability transition following a given action. We shall give the corresponding hierarchical tensor structure for the three functions.

Structure of the v function. We first describe the functional tensor network representation of the d -dimensional value function $v: \mathbb{R}^d \rightarrow \mathbb{R}$. Let $\{\psi_{i;j}\}_{i=1}^n$ denote a collection of orthonormal function basis over a single variable for the j -th co-ordinate, and let $C_v \in \mathbb{R}^{n^d}$ be the tensor represented by a tensor network. The functional tensor network is the d -dimensional function

defined by the following equation:

$$(3.1) \quad v(x) \equiv v(x_1, \dots, x_d) = \sum_{i_1, \dots, i_d=0}^{n-1} (C_v)_{i_1, \dots, i_d} \psi_{i_1;1}(x_1) \cdots \psi_{i_d;d}(x_d) = \left\langle C_v, \bigotimes_{j=1}^d \vec{\Psi}_j(x_j) \right\rangle,$$

where $\vec{\Psi}_j(x_j) = [\psi_{1;j}(x_j), \dots, \psi_{n;j}(x_j)]$ is an n -vector encoding the evaluation for the x_j variable over the entire j -th functional basis. The functional hierarchical tensor structure of v is determined by the hierarchical tensor network ansatz of the tensor C_v .

A hierarchical tensor network is characterized by a hierarchical bipartition of the variable set. The exposition and notations largely follow from [45]. Without loss of generality, let $d = 2^L$ so that the variable set admits exactly L levels of variable bipartition. As illustrated in Figure 1, at the l -th level, the variable index set is partitioned according to

$$(3.2) \quad [d] = \bigcup_{k=1}^{2^l} I_k^{(l)}, \quad I_k^{(l)} := \{2^{L-l+1}(k-1) + 1, \dots, 2^{L-l+1}k\},$$

which in particular implies the recursive relation that $I_k^{(l)} = I_{2k-1}^{(l+1)} \cup I_{2k}^{(l+1)}$. Given the hierarchical bipartition, the tensor network structure of a hierarchical tensor network has the same tree structure as in the variable bipartition, which is illustrated by Figure 1. In short, each internal bond of the tensor network is associated with an edge in the hierarchical binary decomposition, and each physical index is at the leaf node.

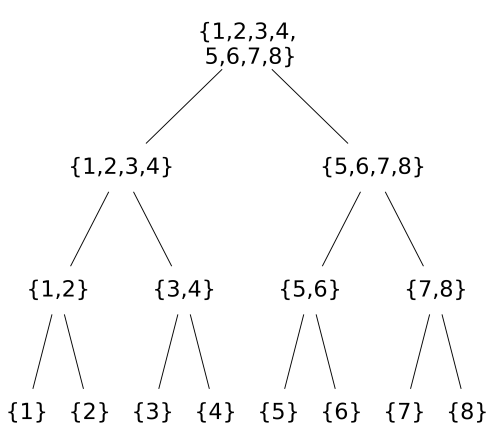
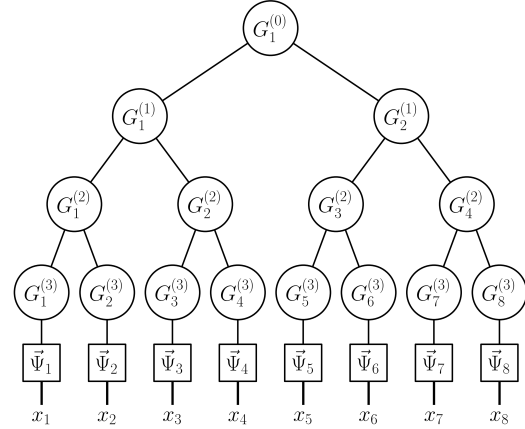


FIG. 1. *Binary decomposition of variables*

FIG. 2. *Functional hierarchical tensor structure of the value function*

Structure of the Q function. The input to the action-value function is the state-action pair, i.e., the concatenation of the d -dimensional state variable (x_1, \dots, x_d) and the m -dimensional control variable (a_1, \dots, a_m) . Similar to the case of representing the value function, we propose to use a binary tree structure for the functional hierarchical tensor structure of the action-value function Q . In this case, one needs to modify the placement of physical bonds to account for the added control variable. We propose to place physical bonds on the non-leaf nodes of the binary tree, one for each of the control variables. As tensor network models are universal approximations, non-optimal placement of variables can still enjoy good performance via suitably increasing the bond dimensions. In our numerical example, we consider the case of $m = 1$, and therefore it is natural to place the physical bond at the root node of the binary tree, illustrated in Figure 3. We note that the proposed approach is heuristic, and the placement of control variables should be determined based on the specific structure of the problem at hand.



Structure of the Markov operator. The Markov operator P is defined such that $P(x, x', a)$ defines the transition probability from state x to x' given one applies the action a . The FHT structure of the Markov operator needs to be consistent with the FHT structure of the action-value function. The physical bonds for the x, x' variable are on the $(L + 1)$ -th level of the binary tree ordered by the interlacing scheme $z = (x_1, x'_1, \dots, x_d, x'_d)$. For the a variable, the placement of the physical bond is on the top $L - 1$ levels, and the location of each physical bond is the same as the respective location for the action-value function. In the case where $m = 1$, one places the physical bond in the root node, illustrated in Figure 4. We note that this network structure is similar to the Markov operator structure in [44].

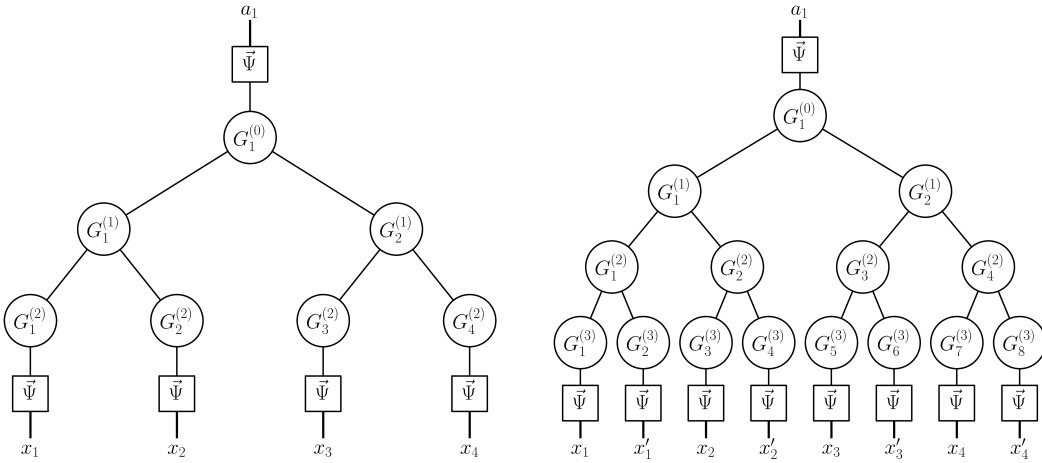


FIG. 3. Functional hierarchical tensor structure of the action-value function for $d = 4, m = 1$.

FIG. 4. Functional hierarchical tensor structure of the Markov operator for $d = 4, m = 1$.

4. Obtain value and action-value functions under the FHT ansatz. This section details the procedure for obtaining the FHT ansatz for the Q and v functions. Section 4.1 introduces the approach for Q function initialization with the Markov operator. Section 4.2 goes through the approach for Q function regression. Section 4.3 explains how to obtain the v function. Section 4.4 details how to use the Q function to form optimal control.

4.1. Action-dependent Markov operator for Q function initialization. One key component to the success of obtaining the action-value function approximation lies in a successful initialization. Here, we propose to use the Markov operator to obtain an initial value of the action-value function. The procedure employs a hierarchical sketching subroutine, as introduced in [44].

The expected cumulative cost for the state-action pair satisfies the following equation:

$$Q_k(x, a) = \mathbb{E} \left[\int_{s=t_k}^{t_{k+1}} f(X_s, a) ds + v(X_{t_{k+1}}, t_{k+1}) \mid (X_{t_k} = x) \wedge (\forall s \in [t_k, t_{k+1}], a_s = a) \right].$$

To obtain an approximation of Q_k , we define the *Markov operator* P by the following equation:

$$P(x, x', a) = \mathbb{P} [X_{t_{k+1}} = x' \mid (X_{t_k} = x) \wedge (\forall s \in [t_k, t_{k+1}], a_s = a)],$$

and so P is the transition probability from x to x' under the constant control a . When $\delta t = t_{k+1} - t_k$ is sufficiently small, one can take the approximation $f(X_s, a) \approx f(X_t, a)$ in conjunction with the Bayes' rule to obtain the following equation:

$$Q_k(x, a) \approx \int_{x'} P(x, x', a) v(x', t_{k+1}) dx' + f(x, a) \delta t,$$

which only introduces an order δt^2 error. Thus, one can see that modelling $Q(x, a)$ can be performed by an integration formula between P and $v(\cdot, t_{k+1})$. Similar to [44], we propose to model P as a functional hierarchical tensor operator. Suppose that g, P has the structure as given in Section 3 respectively, and then the integration between them can be done by efficient tensor contractions. By construction, the contraction of P, g has an FHT ansatz with the same structure proposed for the Q function.

We now describe how the FHT-based approximation of P is obtained. Similar to the construction in [44], we propose to approximate P with the Bayes rule. We let X, O be random state-action pairs following a chosen initial distribution $(X, O) \sim p_0$, and we let X' be the random variable formed by applying a constant control O from state X under the dynamics in Equation (1.2) for a duration of δt . One has

$$(4.1) \quad P(x, x', a) = \frac{1}{p_0(x, a)} \mathbb{P}[X = x, X' = x', O = a],$$

which shows that the conditional density P can be characterized through the probability density of the joint variable (X, X', O) . In our case, the state-action pair is supported on the bounded set $\mathcal{X} \times A$, and it is natural to take $p_0 = \text{Unif}(\mathcal{X} \times A)$. The uniform distribution leads to the formula

$$(4.2) \quad P(x, x', a) = \text{Vol}(\mathcal{X} \times A) \mathbb{P}[X = x, X' = x', O = a],$$

and the joint density $\mathbb{P}[X = x, X' = x', O = a]$ can be obtained by density estimation on the random variable (X, X', O) under the FHT structure described in Section 3. As the approach is only a simple modification of the hierarchical sketching of the FHT ansatz in [44], we include the implementation detail in Appendix C.

4.2. Q function regression under Bellman consistency error. After the action-value function Q_k is initialized, we can take the approach explained in Section 2 to refine the quality of action-value functions through alternating minimization. By selecting a collection of state-action pairs $\{x^{(i)}, a^{(i)}\}_{i=1}^N$, one evolves the dynamics in Equation (1.2) and obtain training samples $\{x^{(i)}, a^{(i)}, (x')^{(i)}, r^{(i)}\}_{i=1}^N$ for the downstream regression task.

Similar to the observations in [34], experiments show that using regression-based loss is not numerically quick to converge for practical problems. Therefore, we propose to use further smoothness regularization. In this case, the samples are normalized so that one has $\{x^{(i)}, a^{(i)}\} \in [-1, 1]^{d+1}$. For the regularization, we use the induced norm of the $(d+1)$ -way tensor product of the Sobolev space $H^1([-1, 1]) \otimes \dots \otimes H^1([-1, 1])$, the details of which can be found in Appendix A. We denote the norm as $\|\cdot\|_{\text{mix}}$. The Sobolev-regularized Q -learning procedure for Q_k has the following loss function:

$$(4.3) \quad L_\mu(Q) = \frac{1}{N} \sum_{i=1}^N \left\| Q(x^{(i)}, a^{(i)}) - v((x')^{(i)}, t_k) - r^{(i)} \right\|_2^2 + \mu \|Q\|_{\text{mix}}^2.$$

We note that the mixed Sobolev norm $\|\cdot\|_{\text{mix}}^2$ is also used in [34], where it serves as a regularization term to promote smoothness in the resulting function. The regularization parameter μ in Equation (4.3) is obtained by cross-validation, and a general rule is that μ is such that the regularization term remains smaller than the regression loss term by orders of magnitude.

Optimization procedure. In this work, we use the alternating least-squares (ALS) method [21] to optimize over the loss in Equation (4.3). An important observation is that the mixed Sobolev norm term $\|Q\|_{\text{mix}}^2$ has a separable structure and admits an efficient tensor diagram. Therefore, the loss function in Equation (4.3) is quadratic in each tensor component. The ALS method takes advantage of the fact that the action-value function Q is parameterized in a multi-linear fashion, and the loss function L_μ is a quadratic function when restricted to each tensor component. Therefore, the ALS method iteratively chooses tensor components and takes minimization over the loss function L_μ . Efficient implementation of the ALS scheme relies on reusing intermediate results on relevant tensor diagrams. By using a node schedule derived from the depth-first-search, one can ensure an efficient implementation where one optimizes over all of the tensor components with $O(d)$ time. The complete implementation details are included in Appendix A.

Selection of training samples. Similar to conventional supervised learning, the selection of the state-action pairs determines the quality of the action-value function. In this work, we use a simple sampling strategy whereby the samplings of states and actions are independent. The action a is sampled from a uniform distribution $a \sim \text{Unif}(A)$. For the state variable x , half of the state samples x are sampled uniformly from \mathcal{X} , and the other half is sampled from the dynamics in Equation (1.2) with $a = 0$. This sampling strategy ensures that there is training data for control-free trajectories. A more refined sampling strategy might lead to better performance.

4.3. Obtaining the v function. After obtaining the action-value function Q_k , obtaining the value function v_k falls within the category of function interpolation. For the action-value function Q_k , we assume that the evaluation $g(x) = \min_a Q_k(x, a)$ is efficient. As one can query the gradient $\nabla_a Q_k(x, a)$ given the FHT ansatz of Q_k , one can also use any conventional first-order optimization procedures (see [30] for an overview). In our work, the numerical experiments consider the case in which a is one-dimensional, in which case any conventional optimization routine is sufficient to obtain the minimum.

Initialization of the v function via hierarchical sketching. To obtain an initialization of the value function, one important subroutine used in this work is functional hierarchical tensor interpolation. Through $v_k(x) = \min_{\hat{a} \in A} Q_k(x, \hat{a})$, one can perform evaluation of v_k . In essence, one performs repeated evaluations of v_k to obtain a sketched linear equation for the tensor component of the FHT structure of v_k . The procedure is a novel use of the hierarchical sketching algorithm [35, 45]. Details are in Appendix B.

Alternating minimization for the v function. After initialization, one selects a collection of state variables $\{x^{(i)}\}_{i=1}^N$, and one calculates the value function target by $y^{(i)} = \min_a Q_k(x^{(i)}, a)$. The fine-tuned value function v_k is obtained by optimizing over the following Sobolev-regularized regression problem:

$$(4.4) \quad L_\mu(v_k) = \frac{1}{N} \sum_{i=1}^N \left\| v_k(x^{(i)}) - y^{(i)} \right\|_2^2 + \mu \|v_k\|_{\text{mix}}^2.$$

Similar to the case of the action-value function, choosing the state variable sample determines the quality of the value function one obtains. For simplicity, this work uses the state variable samples from the state-action pair samples obtained in Subsection 4.2.

4.4. Generating stochastic optimal control with FHT ansatz. After one obtains the collection of action-value functions $\{Q_k\}_{k=0}^{K-1}$, one can use the forward propagation strategy to apply optimal control. At time $t = t_k$, suppose that a particle is at state x . With the strategies proposed in Subsection 4.3, one obtains the optimal control via $a = \arg \min_{\hat{a}} Q_k(x, \hat{a})$, and one can evolve the dynamics with the fixed control a for $\delta t = t_{k+1} - t_k$. One then evolves the dynamics following the aforementioned strategy until one reaches $t = T$.

5. Numerical experiment. We apply the proposed method to a discretized Ginzburg-Landau model in 1D and 2D. For both experiments, the total time is $T = 1$, and we take $K = 10$ time steps with $t_k = \frac{k}{10}$ for $k = 0, \dots, 10$.

We describe the stochastic control problem considered for this case. For 1D and 2D Ginzburg-Landau models, the control-free (i.e. $a = 0$) stochastic dynamics has two meta-stable states $y_+ = (1, \dots, 1)$ and $y_- = (-1, \dots, -1)$. We consider a stabilization task in which one applies control to the stochastic dynamics so that a particle is stabilized around the origin point $(0, \dots, 0)$. Furthermore, we consider the coarse control case in which the control variable is one-dimensional with $A = [-1, 1]$.

To model this, we take the following cost functional:

$$(5.1) \quad J(t, y; (a_s)_{s \in [t, 1]}) = \mathbb{E} \left[\int_{s=t}^1 \frac{1}{d} \|X_s\|^2 + \|a_s\|^2 ds + \frac{1}{d} \|X_1\|^2 \mid X_t = y \right],$$

which means that the instantaneous running cost f satisfies $f(x, a) = \frac{1}{d} \|x\|^2 + \|a\|^2$ and the terminal cost h satisfies $h(y) = \frac{1}{d} \|y\|^2$. Thus, the model is set up so that the terminal cost and

the instantaneous running cost depend on the particle's distance from the origin point $(0, \dots, 0)$, and the instantaneous cost also has a quadratic term in the control variable a .

For the strength of diffusion, we take $\beta = 1$, which makes the effect of diffusion significant without dominating the drift term coming from the Ginzburg-Landau functional.

5.1. Implementation detail.

Initialization strategy. In principle, the Markov operator initialization scheme for the action-value function and the FHT black-box interpolation algorithm for the value function can be used to initialize an FHT ansatz for any $k = 0, \dots, K - 1$. In practical implementations, we use the proposed initialization scheme for initializing the action-value function and the value function only for $k = K - 1$. Subsequent initialization is done by initializing the FHT ansatz Q_k, v_k with that of Q_{k+1}, v_{k+1} . As $t_{k+1} - t_k$ is small in our case, one has $v_{k+1} \approx v_k$ and $Q_{k+1} \approx Q_k$. By doing so, the cost for the more involved initialization procedure only needs to occur once for each ansatz, which simplifies the procedure while maintaining numerical accuracy.

The choice of basis function. Similar to [44], the $\int_z |1-x(z)|^2 dz$ term in the Ginzburg-Landau functional and the $\|X_s\|^2$ term in the cost functional effectively ensures that the trajectory of a particle under an optimal trajectory is bounded within the domain $[-2, 2]^d$, which is why we take the domain to be the region $\mathcal{X} = [-2, 2]^d$. Therefore, for the state variable x , we use the polynomial representation by choosing a maximal degree parameter q and picking the first $n = q + 1$ Legendre basis polynomial in $[-2, 2]$. For the control variable a , we similarly use the first n Legendre basis polynomial in $A = [-1, 1]$. In particular, we choose $q = 6$. The effect of Sobolev-type regularization in Equation (4.3) implies that the presence of low-degree polynomials is more prevalent, which is why $q = 6$ is sufficient in this case.

Bipartition structure. The bipartition structure for the state variable exactly follows that of [45], and we give an overview here for completeness. Assume for simplicity that a function x in Δ -dimensions is discretized to the $d = m^\Delta$ points denoted $\{x_{i_1, \dots, i_\Delta}\}_{i_1, \dots, i_\Delta \in [m]}$ with $m = 2^\mu$. For each index i_δ , one performs a length μ binary expansion $i_\delta = a_{\delta 1} \dots a_{\delta \mu}$. The variable x_{i_1, \dots, i_Δ} is given index k with the length $\mu\Delta$ binary expansion $k = a_{11}a_{21} \dots a_{\Delta-1, \mu}a_{\Delta, \mu}$, and the associated binary decomposition structure follows from the given index according to Equation (3.2). For other stochastic control problems, one can design a bipartition structure to fit the relationship between the variables.

Alternating minimization. In the proposed alternating-least-squares (ALS) approach, one performs minimization over the tensor components once for each sweep schedule. One question is how many rounds of ALS are sufficient for the regression to be successful, as the Bellman consistency loss is a regression problem with noisy labels, and the model is under-parameterized. In general, one can use the typical regression strategy in supervised learning, where one performs training until the loss function does not improve. In our case, for every time step t_k , we use five rounds of ALS for both the action-value function and the value function, which is sufficient for convergence. We remark that the success of ALS is heavily attributed to the initialization strategy proposed, and otherwise ALS cannot guarantee efficiency in training.

5.2. 1D Ginzburg-Landau model. We first consider a 1D Ginzburg-Landau model. The potential energy is defined as

$$(5.2) \quad V(x_1, \dots, x_m) := \left[\frac{\lambda}{2} \sum_{i=1}^{m+1} \left(\frac{x_i - x_{i-1}}{h} \right)^2 + \frac{\mu}{4} \sum_{i=1}^m (1 - x_i^2)^2 \right] h,$$

where $h = \frac{1}{m+1}$ and $x_0 = x_{m+1} = 0$. In particular, we fix $m = 64$, $\lambda = 0.2$, $\mu = 1$. The dimension is $d = 64$. For the control variable, we take a vector $\omega \in \mathbb{R}^d$ where we let $\omega_i = 1$ if $\frac{i}{d} \in [0.25, 0.6]$, and $\omega_i = 0$ otherwise. This is a discretization of the situation where one can apply a one-dimensional perturbation in the direction of $\omega = \mathbf{1}_{[0.25, 0.6]}$. The drift term b admits the form

$$b(x, a) = -\nabla V(x) + 20a\omega,$$

and the cost functional J follows the form in Equation (5.1).

In the first numerical test, we test whether a randomly generated particle can go to the origin instead of one of the meta-stable states y_+, y_- . To test performance, we first generate 500 particles from the uniform distribution of $\mathcal{X} = [-2, 2]^d$. In addition, we sample along another 500 points along the line segment $I = \{(t, t, \dots, t) \mid t \in (-2, 2)\}$ from the uniform distribution on I . In Figure 5, we plot the concentration of the 1000 particles after applying locally constant stochastic control generated by the action-value functions. One can see that the FHT-based action-value function is successful at generating a control policy that guides the randomly generated particles to the origin.

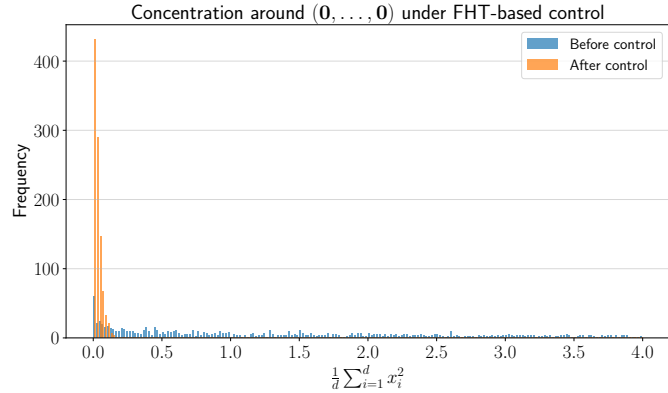


FIG. 5. 1D Ginzburg-Landau model. Distribution of the normalized distance of particles from the origin point. One can see that the proposed method succeeds at stabilizing a particle around the origin.

In the second numerical test, we test the accuracy of the action-value function the proposed method obtains. In particular, we consider the accuracy for the action-value function at time $t = t_{K-1}$. This choice is because one can obtain the ground truth action-value function for any state-action pair by simply using Monte Carlo simulation. For illustration, we plot the action-value function $Q_{K-1}(x, a)$ for varying values of a at two points $x = y_+$ and $x = y_-$. These two points are representative as the control-free trajectory stabilizes at the two meta-stable states, and it is desirable if the ansatz can form the optimal control from the two points accurately. In Figure 6, we plot the action-value function $Q_k(x, a)$ for $x = y_+$ and y_- , which shows that the FHT approximation is very accurate. For both cases, the average relative error is 1.6%. Importantly, one can see that the Sobolev regularization ensures that the action-value function is smooth across action values, which is appealing when one needs to use a first-order optimization approach to find $\arg \min_a Q(x, a)$. The accuracy is similar when one chooses other values of x , where we observe that the action-value function estimation remains accurate.

In the third numerical test, we test the accuracy of the value function. Unlike the case for the action-value function, one does not have a ground-truth reference for the value function. Therefore, we similarly consider $t = t_{K-1}$, and we propose to test the accuracy of v_{K-1} as the expected cumulative cost for the policy one forms using the action-value function at $t = t_{K-1}$. In particular, we pick $N = 600$ points, from which 300 points come from the uniform distribution of $\mathcal{X} = [-2, 2]^d$, and the other 300 points come from the uniform distribution of the line segment $I = \{(t, t, \dots, t) \mid t \in (-2, 2)\}$. For each point, we sample 100 SDE trajectories following the optimal trajectories obtained from Q_{K-1} , and we use the average cumulative cost to form the Monte-Carlo reference. As can be seen from Figure 7, the value function v_{K-1} matches well with references, and so the value function prediction is quite accurate. The results for other time steps are similar.

5.3. 2D Ginzburg-Landau model. We then consider a 2D Ginzburg-Landau model. The potential energy follows from Equation (1.6). In particular, we fix $m = 8$, $\lambda = 0.5$, $\mu = 1$. The dimension is $d = 64$. For the control variable, we take a vector $\omega \in \mathbb{R}^d$ where we let $\omega_{(i,j)} = 1$ if $(\frac{i}{d}, \frac{j}{d}) \in [0.2, 0.8]^2$, and $\omega_{(i,j)} = 0$ otherwise. This is a discretization of the situation where one can

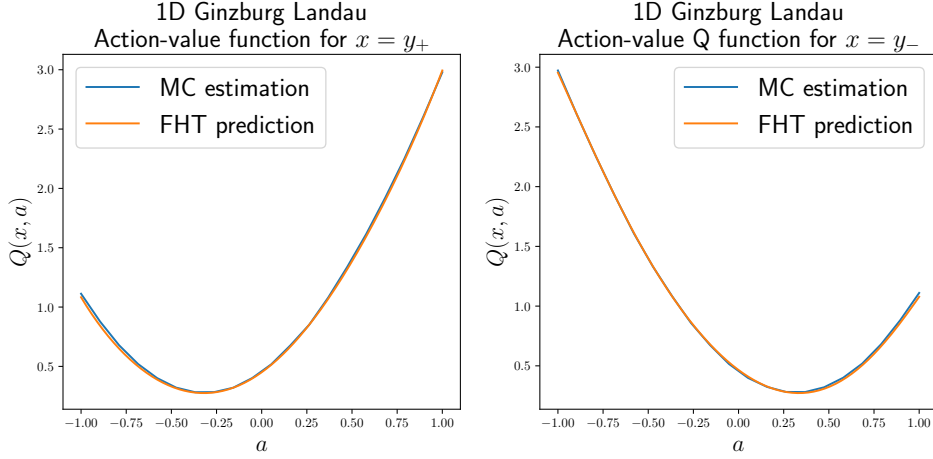


FIG. 6. 1D Ginzburg-Landau model. Plot of the action-value function at time $t = t_{K-1}$. The ground truth action-value function is obtained through Monte-Carlo simulation.

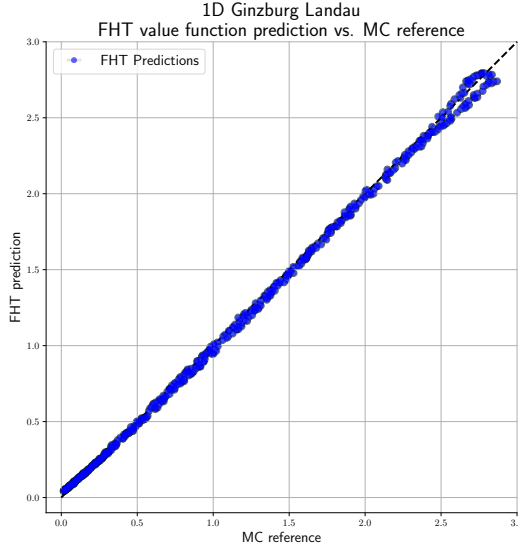


FIG. 7. 1D Ginzburg Landau model. Plots of the function evaluation of the FHT-based approximation of the value function at randomly sampled points. The reference values are obtained from Monte-Carlo estimations.

apply a one-dimensional perturbation in the direction of $\omega = \mathbf{1}_{[0.2, 0.8]^2}$. The drift term b admits the form

$$b(x, a) = -\nabla V(x) + 20a\omega,$$

and the cost functional J follows the form in Equation (5.1).

We perform three numerical tests under the same setting as the 1D tests. In Figure 8 we show the concentration of 1000 particles (500 generated from the uniform distribution of $\mathcal{X} = [-2, 2]^d$ and 500 along the line segment $I = \{(t, t, \dots, t) \mid t \in (-2, 2)\}$) after applying locally constant stochastic control generated by the action-value functions. One can see that the FHT-based action-value function successfully takes the particles to the region around the origin. In Figure 9, we plot the action-value function at the two meta-stable states y_+, y_- . The results show that the FHT approximate action-value function is close to the Monte-Carlo reference, and the average

relative error in both cases is smaller than 3.4%. The results for other state values are similar. In Figure 10, we plot the value function compared to Monte Carlo references. The results show that the value function prediction similarly has good performance.

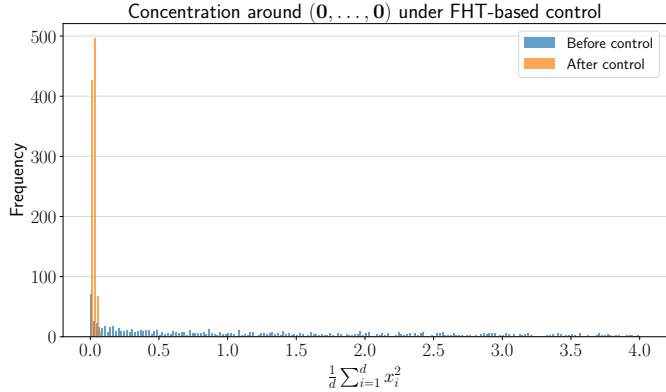


FIG. 8. 2D Ginzburg-Landau model. Distribution of the normalized distance of particles from the origin point. One can see that the proposed method succeeds at stabilizing a particle around the origin.

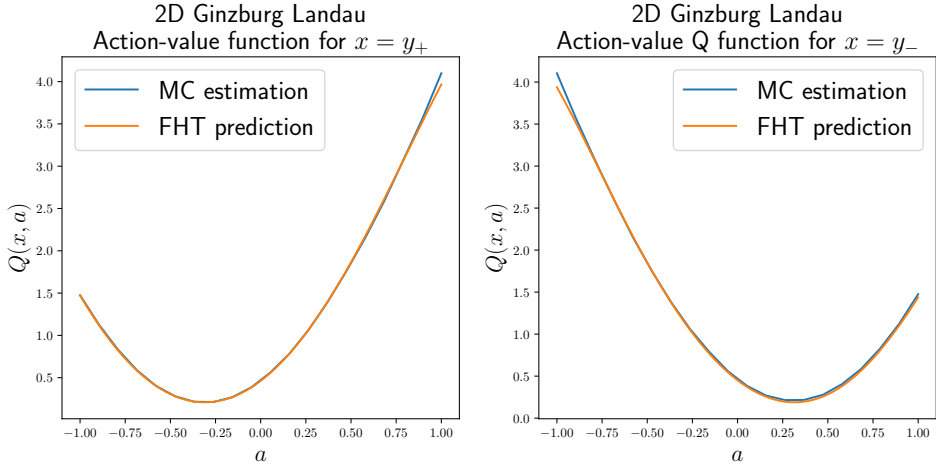


FIG. 9. 2D Ginzburg-Landau model. Plot of the action-value function at time $t = t_{K-1}$. The ground truth action-value function is obtained through Monte-Carlo simulation.

6. Conclusion. We introduce a novel strategy to solve the Hamilton-Jacobi-Bellman equation with a functional hierarchical tensor network ansatz. The algorithm is applied to two problems with a discretized Ginzburg-Landau functional in 1D and 2D. This method demonstrates the effectiveness and high accuracy of using tensor-network-based methods to tackle high-dimensional PDEs.

REFERENCES

- [1] A. BACHOUCH, C. HURÉ, N. LANGRENÉ, AND H. PHAM, *Deep neural networks algorithms for stochastic control problems on finite horizon: Numerical applications*, Methodology and Computing in Applied Probability, 24 (2022), pp. 143–178.
- [2] R. W. BEARD, *Successive galerkin approximation algorithms for nonlinear optimal and robust control*, International Journal of Control, 71 (1998), pp. 717–743.

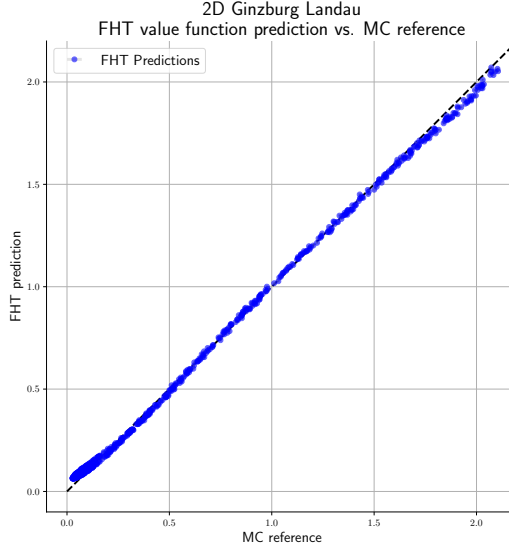


FIG. 10. *2D Ginzburg Landau model. The plot of the function evaluation of the FHT-based approximation of the value function at randomly sampled points. The reference values are obtained from Monte-Carlo estimations.*

- [3] R. W. BEARD, G. N. SARIDIS, AND J. T. WEN, *Galerkin approximations of the generalized Hamilton-Jacobi-Bellman equation*, *Automatica*, 33 (1997), pp. 2159–2177.
- [4] S. CHEN, X. LI, AND X. Y. ZHOU, *Stochastic linear quadratic regulators with indefinite control weight costs*, *SIAM Journal on Control and Optimization*, 36 (1998), pp. 1685–1702.
- [5] Y. CHEN AND Z. LU, *Tensor decomposition and high-performance computing for solving high-dimensional stochastic control system numerically*, *Journal of Systems Science and Complexity*, 35 (2022), pp. 123–136.
- [6] J. DARBON AND T. MENG, *On some neural network architectures that can represent viscosity solutions of certain high dimensional Hamilton-Jacobi partial differential equations*, *Journal of Computational Physics*, 425 (2021), p. 109907.
- [7] S. DOLGOV, D. KALISE, AND K. K. KUNISCH, *Tensor decomposition methods for high-dimensional Hamilton-Jacobi-Bellman equations*, *SIAM Journal on Scientific Computing*, 43 (2021), pp. A1625–A1650.
- [8] S. DOLGOV, D. KALISE, AND L. SALUZZI, *Data-driven tensor train gradient cross approximation for hamilton-jacobi-bellman equations*, *SIAM Journal on Scientific Computing*, 45 (2023), pp. A2153–A2184.
- [9] W. E, J. HAN, AND A. JENTZEN, *Deep learning-based numerical methods for high-dimensional parabolic partial differential equations and backward stochastic differential equations*, *Communications in Mathematics and Statistics*, 5 (2017), pp. 349–380.
- [10] M. EIGEL, R. SCHNEIDER, AND D. SOMMER, *Dynamical low-rank approximations of solutions to the Hamilton-Jacobi-Bellman equation*, *Numerical Linear Algebra with Applications*, 30 (2023), p. e2463.
- [11] K. FACKELDEY, M. OSTER, L. SALLANDT, AND R. SCHNEIDER, *Approximative policy iteration for exit time feedback control problems driven by stochastic differential equations using tensor train format*, *Multiscale Modeling & Simulation*, 20 (2022), pp. 379–403.
- [12] P. FORSYTH AND G. LABAHN, *Numerical methods for controlled Hamilton-Jacobi-Bellman PDEs in finance*, *The Journal of Computational Finance*, 11 (2007), pp. 1–43.
- [13] A. GORODETSKY, S. KARAMAN, AND Y. MARZOUK, *Efficient high-dimensional stochastic optimal motion control using tensor-train decomposition*, in *Robotics: Science and Systems XI*, Robotics: Science and Systems Foundation, 2015.
- [14] A. GORODETSKY, S. KARAMAN, AND Y. MARZOUK, *High-dimensional stochastic optimal control using continuous tensor decompositions*, *The International Journal of Robotics Research*, 37 (2018), pp. 340–377.
- [15] T. HAARNOJA, A. ZHOU, P. ABBEEL, AND S. LEVINE, *Soft actor-critic: Off-policy maximum entropy deep reinforcement learning with a stochastic actor*, in *International conference on machine learning*, PMLR, 2018, pp. 1861–1870.
- [16] W. HACKBUSCH, *Tensor spaces and numerical tensor calculus*, vol. 42, Springer, 2012.
- [17] W. HACKBUSCH AND S. KÜHN, *A new scheme for the tensor representation*, *Journal of Fourier analysis and applications*, 15 (2009), pp. 706–722.
- [18] J. HAN AND W. E, *Deep learning approximation for stochastic control problems*, arXiv preprint arXiv:1611.07422, (2016).
- [19] J. HAN, A. JENTZEN, AND W. E, *Solving high-dimensional partial differential equations using deep learning*, *Proceedings of the National Academy of Sciences*, 115 (2018), pp. 8505–8510.
- [20] M. HAN, L. ZHANG, J. WANG, AND W. PAN, *Actor-critic reinforcement learning for control with stability*

guarantee, *IEEE Robotics and Automation Letters*, 5 (2020), pp. 6217–6224.

[21] S. HOLTZ, T. ROHWEDDER, AND R. SCHNEIDER, *The alternating linear scheme for tensor optimization in the tensor train format*, *SIAM Journal on Scientific Computing*, 34 (2012), pp. A683–A713.

[22] M. B. HOROWITZ, A. DAMLE, AND J. W. BURDICK, *Linear Hamilton Jacobi Bellman equations in high dimensions*, in 53rd IEEE Conference on Decision and Control, IEEE, 2014, pp. 5880–5887.

[23] Z. HU, K. SHUKLA, G. E. KARNIADAKIS, AND K. KAWAGUCHI, *Tackling the curse of dimensionality with physics-informed neural networks*, *Neural Networks*, 176 (2024), p. 106369.

[24] D. KALISE AND K. KUNISCH, *Polynomial approximation of high-dimensional Hamilton–Jacobi–Bellman equations and applications to feedback control of semilinear parabolic PDEs*, *SIAM Journal on Scientific Computing*, 40 (2018), pp. A629–A652.

[25] V. KONDA AND J. TSITSIKLIS, *Actor-critic algorithms*, *Advances in neural information processing systems*, 12 (1999).

[26] T. LIU, S. DING, J. ZHANG, AND L. ZHOU, *Pinn-based viscosity solution of HJB equation*, arXiv preprint arXiv:2309.09953, (2023).

[27] A. MOSSKULL AND K. M. ARFVIDSSON, *Solving the Hamilton–Jacobi–Bellman equation for route planning problems using tensor decomposition*, 2020.

[28] T. NAKAMURA-ZIMMERER, Q. GONG, AND W. KANG, *A causality-free neural network method for high-dimensional Hamilton–Jacobi–Bellman equations*, in 2020 American Control Conference (ACC), 2020, pp. 787–793.

[29] T. NAKAMURA-ZIMMERER, Q. GONG, AND W. KANG, *Adaptive deep learning for high-dimensional Hamilton–Jacobi–Bellman equations*, *SIAM Journal on Scientific Computing*, 43 (2021), pp. A1221–A1247.

[30] J. NOCEDAL AND S. J. WRIGHT, *Numerical optimization*, Springer, 1999.

[31] N. NÜSKEN AND L. RICHTER, *Solving high-dimensional Hamilton–Jacobi–Bellman PDEs using neural networks: perspectives from the theory of controlled diffusions and measures on path space*, *Partial Differential Equations and Applications*, 2 (2021), p. 48.

[32] I. OSELEDETS AND E. TYRTYSHNIKOV, *Tt-cross approximation for multidimensional arrays*, *Linear Algebra and its Applications*, 432 (2010), pp. 70–88.

[33] M. OSTER, L. SALLANDT, AND R. SCHNEIDER, *Approximating the stationary Bellman equation by hierarchical tensor products*, arXiv preprint arXiv:1911.00279, (2019).

[34] M. OSTER, L. SALLANDT, AND R. SCHNEIDER, *Approximating optimal feedback controllers of finite horizon control problems using hierarchical tensor formats*, *SIAM Journal on Scientific Computing*, 44 (2022), pp. B746–B770.

[35] Y. PENG, Y. CHEN, E. M. STOUDENMIRE, AND Y. KHOO, *Generative modeling via hierarchical tensor sketching*, arXiv preprint arXiv:2304.05305, (2023).

[36] H. PHAM, X. WARIN, AND M. GERMAIN, *Neural networks-based backward scheme for fully nonlinear PDEs*, *SIAM Journal on Numerical Analysis*, 59 (2021), pp. 1–16.

[37] A. RAO, *A survey of numerical methods for optimal control*, *Advances in the Astronautical Sciences*, 135 (2009), pp. 497–528.

[38] S. RICHARDSON AND S. WANG, *Numerical solution of Hamilton–Jacobi–Bellman equations by an exponentially fitted finite volume method*, *Optimization*, 55 (2006), pp. 121–140.

[39] R. SCHNEIDER AND A. USCHMAJEW, *Approximation rates for the hierarchical tensor format in periodic Sobolev spaces*, *Journal of Complexity*, 30 (2014), pp. 56–71.

[40] S. SHETTY, T. XUE, AND S. CALINON, *Generalized policy iteration using tensor approximation for hybrid control*, in The Twelfth International Conference on Learning Representations, 2024.

[41] T. SHI, D. HAYES, AND J.-M. QIU, *Distributed memory parallel adaptive tensor-train cross approximation*, arXiv preprint arXiv:2407.11290, (2024).

[42] D. SOMMER, R. GRUHLKE, M. KIRSTEIN, M. EIGEL, AND C. SCHILLINGS, *Generative modelling with tensor train approximations of Hamilton–Jacobi–Bellman equations*, arXiv preprint arXiv:2402.15285, (2024).

[43] R. S. SUTTON AND A. G. BARTO, *Reinforcement learning: An introduction*, MIT press, 2018.

[44] X. TANG, L. COLLIS, AND L. YING, *Solving high-dimensional kolmogorov backward equations with functional hierarchical tensor operators*, *SIAM Journal on Scientific Computing*, 47 (2025), pp. A613–A632.

[45] X. TANG AND L. YING, *Solving high-dimensional fokker-planck equation with functional hierarchical tensor*, *Journal of Computational Physics*, 511 (2024), p. 113110.

[46] H. VAN HASSELT, A. GUEZ, AND D. SILVER, *Deep reinforcement learning with double Q-learning*, in Proceedings of the AAAI conference on artificial intelligence, vol. 30, 2016.

[47] S. WANG, L. JENNINGS, AND K. TEO, *Numerical solution of Hamilton–Jacobi–Bellman equations by an upwind finite volume method*, *Journal of Global Optimization*, 27 (2003), pp. 177–192.

[48] S. WANG, L. S. JENNINGS, AND K. L. TEO, *Numerical solution of Hamilton–Jacobi–Bellman equations by an upwind finite volume method*, *Journal of Global Optimization*, 27 (2003), pp. 177–192.

[49] T. WANG, H. ZHANG, AND Y. LUO, *Stochastic linear quadratic optimal control for model-free discrete-time systems based on Q-learning algorithm*, *Neurocomputing*, 312 (2018), pp. 1–8.

[50] C. J. C. H. WATKINS, *Learning from delayed rewards*, King's College, Cambridge United Kingdom, 1989.

[51] J. YONG AND X. Y. ZHOU, *Stochastic controls: Hamiltonian systems and HJB equations*, vol. 43, Springer Science & Business Media, 2012.

[52] M. ZHOU, J. HAN, AND J. LU, *Actor-critic method for high dimensional static Hamilton–Jacobi–Bellman partial differential equations based on neural networks*, *SIAM Journal on Scientific Computing*, 43 (2021), pp. A4043–A4066.

Appendix A. Implementation details of alternating minimization.

In this section, we detail the alternating minimization algorithm used in Subsection 4.2 and Subsection 4.3. Without loss of generality, we discuss the case of g representing the value function, and one can extend to the action-value function case with mild change to the subroutine.

The goal is to find an approximate functional hierarchical tensor representation of a function $g(x)$ such that the following loss term is minimized:

$$(A.1) \quad L_\mu(g) = \frac{1}{N} \sum_{i=1}^N \|g(x^{(i)}) - y^{(i)}\|_2^2 + \mu \|g\|_{\text{mix}}^2,$$

where $\{x^{(i)}, y^{(i)}\}_{i=1}^N$ is the training data set for the Bellman consistency error. For the case of the Q function at $t = t_k$, one takes collected samples of $\{x^{(i)}, a^{(i)}, (x')^{(i)}, r^{(i)}\}_{i=1}^N$ by simulating the trajectory of $x^{(i)}$ under action $a^{(i)}$, and the regression target is $y^{(i)} = r^{(i)} + v((x')^{(i)}, t_{k+1})$. In the case of the v function at $t = t_k$, one takes samples $\{x^{(i)}\}_{i=1}^N$ and the regression target is $y^{(i)} = \min_{a \in A} Q_k(x^{(i)}, a)$.

The mixed Sobolev norm $\|\cdot\|_{\text{mix}}$ is defined by

$$\|f\|_{\text{mix}} = \left(\sum_{k_1=0}^1 \cdots \sum_{k_d=0}^1 \left\| \left(\frac{\partial}{\partial x_1} \right)^{k_1} \cdots \left(\frac{\partial}{\partial x_d} \right)^{k_d} f \right\|^2 \right)^{\frac{1}{2}},$$

where one can see that $\|\cdot\|_{\text{mix}}$ is the norm equipped for the mixed Sobolev space $H_{\text{mix}}^1 \equiv \otimes_{i=1}^d H^1$. Under the functional hierarchical tensor representation, the function g is parameterized by a collection of tensor components. With all but one tensor component fixed, the loss function L_μ in Equation (A.1) is a quadratic function for a single tensor component. In essence, alternating minimization is a greedy approach aiming at solving each tensor node sequentially by minimizing the corresponding local quadratic function, with the goal of reaching the global minimum of Equation (A.1).

We first detail the derivation behind alternating minimization for a single tensor component. We fix a node q that stands for the k -th block at level l of variable bipartition under the FHT ansatz. We consider G_q , which stands for the tensor component corresponding to q , and we show that Equation (A.1) is a quadratic function in G_q . For the rest of this section, we reserve the symbol G to denote the vectorization of G_q , i.e., $G := \text{vec}(G_q)$. For simplicity, we assume the general case $0 < l < L$ so that q is neither the root nor the leaf node.

Bellman consistency error. First we show that the Bellman consistency error $\|g(x^{(i)}) - y^{(i)}\|_2^2$ is a quadratic function of G_q . The function g in the FHT function class admits a representation

$$(A.2) \quad g(x) \equiv g(x_1, \dots, x_d) = \left\langle C, \bigotimes_{j=1}^d \vec{\Psi}_j(x_j) \right\rangle,$$

where $\vec{\Psi}_j$ is the basis set defined in Equation (3.1) and C is the coefficient tensor. The evaluation of g on the collected points $\{x^{(i)}\}_{i=1}^N$ reads $g(x^{(i)}) = \left\langle C, \bigotimes_{j=1}^d \vec{\Psi}_j(x_j^{(i)}) \right\rangle$.

To show how the evaluation of g depends on G_q , we let $a := I_{2k-1}^{(l+1)}$, $b := I_{2k}^{(l+1)}$ and $f = [d] - a \cup b$, where $I_k^{(l)}$ follows hierarchical bipartition introduced in Equation (3.2). The structural low-rankness property of the FHT ansatz implies that there exist $r_a, r_b, r_f \in \mathbb{N}$, $C_a: [n^{|a|}] \times [r_a] \rightarrow \mathbb{R}$, $C_b: [n^{|b|}] \times [r_b] \rightarrow \mathbb{R}$, $C_f: [r_f] \times [n^{|f|}] \rightarrow \mathbb{R}$ such that the following equations hold for $G_q: [r_a] \times [r_b] \times [r_f] \rightarrow \mathbb{R}$:

$$(A.3) \quad C(i_a, i_b, i_f) = \sum_{\alpha, \beta, \theta} C_a(i_a, \alpha) C_b(i_b, \beta) G_q(\alpha, \beta, \theta) C_f(\theta, i_f),$$

where terms such as i_a follows the multi-index notation as defined in Subsection 1.2.

Combining Equation (A.2) and Equation (A.3), one has

$$(A.4) \quad g(x^{(i)}) = \sum_{\alpha, \beta, \theta} A_a(i, \alpha) A_b(i, \beta) A_f(i, \theta) G_q(\alpha, \beta, \theta),$$

where the i -th row of matrices A_a, A_b, A_f is the contraction of C_a, C_b, C_f with $\bigotimes_{j \in a} \vec{\Psi}_j(x_j^{(i)})$, $\bigotimes_{j \in b} \vec{\Psi}_j(x_j^{(i)})$ and $\bigotimes_{j \in f} \vec{\Psi}_j(x_j^{(i)})$. Now, we take the vectorization $G = \text{vec}(G_q)$ and let $A: [N] \times [r_a \times r_b \times r_f] \rightarrow \mathbb{R}$ be the *evaluation matrix* satisfying

$$(A.5) \quad A(i, (\alpha, \beta, \theta)) = A_a(i, \alpha) A_b(i, \beta) A_f(i, \theta),$$

and then one has $\sum_{i=1}^n \|g(x^{(i)}) - y^{(i)}\|_2^2 = \|AG - y\|^2$, which is indeed a quadratic function in the entries of G_q .

Mixed Sobolev regularization. Similarly, we show that the term $\|g\|_{\text{mix}}^2$ is a quadratic function in G_q . When g admits an FHT parameterization in terms of C by Equation (A.2), one has $\|g\|_{\text{mix}}^2 = \text{vec}(C)^\top K \text{vec}(C)$ for an exponentially-sized matrix K . An efficient evaluation of K relies primarily on the fact that K admits a separable tensor product structure. To see this, one can check the action of K on separable functions. For each site $j \in [d]$, one can take an arbitrary function ϕ_j within the vector space spanned by the basis function for the j -th variable x_j . By taking $f := \prod_{j=1}^d \phi_j$, one sees that f is separable in the sense that $f(x_1, \dots, x_d) = \prod_{j=1}^d \phi_j(x_j)$ and

$$\left\| \prod_{j=1}^d \phi_j \right\|_{\text{mix}}^2 = \sum_{k_1=0}^1 \dots \sum_{k_d=0}^1 \left\| \left(\frac{\partial}{\partial x_1} \right)^{k_1} \dots \left(\frac{\partial}{\partial x_d} \right)^{k_d} \prod_{j=1}^d \phi_j \right\|^2 = \sum_{k_1=0}^1 \dots \sum_{k_d=0}^1 \prod_{j=1}^d \left\| \left(\frac{d}{dx} \right)^{k_j} \phi_j \right\|^2,$$

where the second equality holds due to Fubini's theorem. Subsequently, factorizing the exponentially sized summation allows us to rewrite

$$\left\| \prod_{j=1}^d \phi_j \right\|_{\text{mix}}^2 = \prod_{j=1}^d \left\| \sum_{k_j=0}^1 \left(\frac{d}{dx} \right)^{k_j} \phi_j \right\|^2.$$

Thus, the exponential-sized matrix $K: [n_1 \times \dots n_d] \times [n_1 \times \dots n_d] \rightarrow \mathbb{R}$ can be written as a tensor product of matrices $K = K_1 \otimes \dots \otimes K_d$, where $K_j: [n_j] \times [n_j]$ is the matrix defined by

$$K_j(i, i') = \left\langle \sum_{k=0}^1 \left(\frac{d}{dx} \right)^k \psi_{i;j}, \sum_{k'=0}^1 \left(\frac{d}{dx} \right)^{k'} \psi_{i';j} \right\rangle_{L^2([-1,1])}.$$

When restricted to the tensor component G_q , one can likewise show that the Sobolev mixed norm term admits a form $G^\top MG$. Let $K_a = \bigotimes_{j \in a} K_j$, $K_b = \bigotimes_{j \in b} K_j$, $K_f = \bigotimes_{j \in f} K_j$. We form matrices M_a, M_b, M_f by $M_a = C_a^\top K_a C_a, M_b = C_b^\top K_b C_b, M_f = C_f^\top K_f C_f$, where we utilize the matrix structure for C_a, C_b, C_f defined in this section. The term $\|g\|_{\text{mix}}$ can thus be written as $\|g\|_{\text{mix}} = G^\top MG$, where $M: [r_a \times r_b \times r_f] \times [r'_a \times r'_b \times r'_f] \rightarrow \mathbb{R}$ satisfies $M = M_a \otimes M_b \otimes M_f$, i.e.

$$(A.6) \quad M((\alpha, \beta, \theta), (\alpha', \beta', \theta')) = M_a(\alpha, \alpha') M_b(\beta, \beta') M_f(\theta, \theta').$$

Single-node optimization in alternating minimization. Combining with the results above, the quadratic problem for the tensor component G_q is thus

$$\min_G \|AG - y\|_2^2 + \mu G^\top MG.$$

The solution under the single-node optimization procedure is given by

$$(A.7) \quad G_q = \text{Reshape}(G, r_a, r_b, r_f), \quad G = (A^\top A + \mu M)^{-1} A^\top y.$$

For an efficient numerical implementation, an important concept in performing single-node optimization for the FHT ansatz is the *messages* sent to the node q . The messages encapsulate the information necessary to compute the solution in Equation (A.7). For illustration, we let q be the node corresponding to the tensor component $G_1^{(1)}$ in Figure 11 and explain the procedure. To compute G from Equation (A.7), we need to form tensors A_a, A_b, A_f and M_a, M_b, M_f , and these six tensors are the messages to q . For simplicity, we use $m_{G_1^{(2)} \rightarrow G_1^{(1)}}, m_{G_2^{(2)} \rightarrow G_1^{(1)}}, m_{G_1^{(0)} \rightarrow G_1^{(1)}}$ to denote (A_a, M_a) , (A_b, M_b) , (A_f, M_f) respectively in the example. We note that each edge of a functional hierarchical tensor corresponds to two messages in two directions, and there are $O(d)$ messages in total.

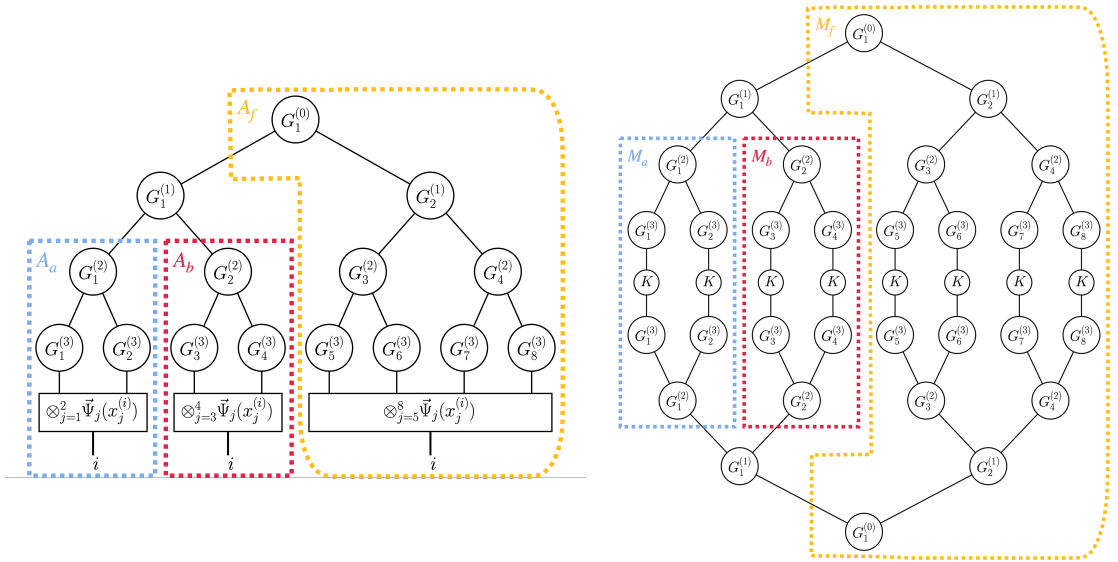


FIG. 11. Left: diagrammatic expression of A_a, A_b, A_f appearing in Equation (A.4) for $G_1^{(1)}$. Right: diagrammatic expression of M_a, M_b, M_f appearing in Equation (A.6) for $G_1^{(1)}$.

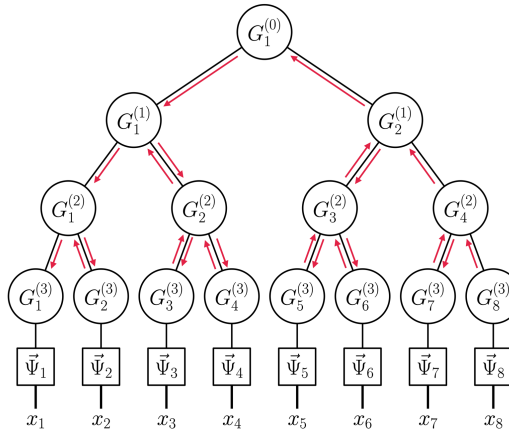


FIG. 12. Depth-first-search path used in the sequential optimization of the functional hierarchical tensor.

Node traversal for efficient alternating minimization. We now go through the procedure for computing the optimal G_q under the alternating minimization procedure. Naively, one could

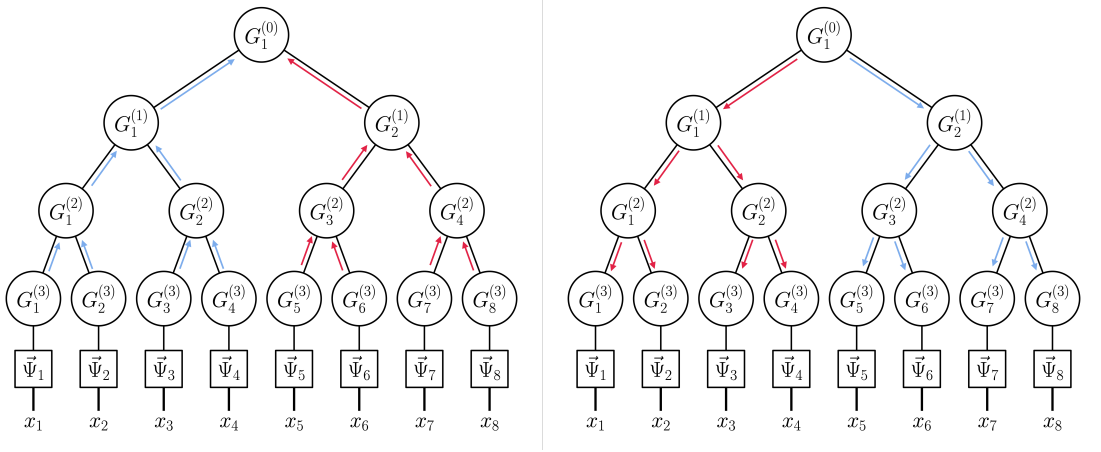


FIG. 13. *Message initialization process. Left: Leaf-to-root sweep process computing all children's messages. Right: Root-to-leaf sweep process computing all parent's messages.*

compute the messages sent to each node q separately by sequential tensor contractions starting from the leaf nodes. It is not hard to see that this procedure would be inefficient, as it requires $O(d)$ operations for updating a specific tensor component, leading to a total complexity of $O(d^2)$ to update all of the tensor components. In this work, we adopt a specific scheduling of tensor components optimization inspired by depth-first-search. The proposed strategy allows one to achieve an $O(d)$ total complexity for node updates. The procedure is illustrated in Figure 12 and Figure 13

Essentially, the proposed update strategy is based on the fact that one can update messages in $O(1)$ cost for its nearest neighbor with a single tensor contraction. Using the example shown in Figure 11, one sees that $m_{G_1^{(1)} \rightarrow G_1^{(2)}}$ can be computed with the knowledge of $m_{G_1^{(0)} \rightarrow G_1^{(1)}}$, $m_{G_2^{(2)} \rightarrow G_1^{(1)}}$ and $G_1^{(1)}$. Specifically, A_f of $G_1^{(2)}$ is given by a tensor contraction of three independent tensors: $G_1^{(1)}$, A_b of $G_1^{(1)}$ and A_f of $G_1^{(1)}$; M_f of $G_1^{(2)}$ is given by a tensor contraction of four independent tensors: $G_1^{(1)}$, $G_1^{(1)}$, M_b of $G_1^{(1)}$ and M_f of $G_1^{(1)}$.

The depth-first-search-inspired schedule we use is illustrated in Figure 12 as a directed walk on the hierarchical tree. We compute all of the messages in the beginning and start the walk from $G_8^{(3)}$. As three required messages are available, the tensor component $G_8^{(3)}$ is optimized via Equation (A.7), and the schedule moves on to $G_4^{(2)}$. To optimize $G_4^{(2)}$, two required messages $m_{G_7^{(3)} \rightarrow G_4^{(2)}}$ and $m_{G_2^{(1)} \rightarrow G_4^{(2)}}$ are up to date. Since $G_8^{(3)}$ has been updated, the message $m_{G_8^{(3)} \rightarrow G_4^{(2)}}$ becomes out of date and one updates the message using the updated $G_8^{(3)}$. Then $G_4^{(2)}$ is optimized using the updated messages to it, and the schedule moves on to $G_7^{(3)}$. To optimize $G_7^{(3)}$, only $m_{G_4^{(2)} \rightarrow G_7^{(3)}}$ is required, but $m_{G_4^{(2)} \rightarrow G_7^{(3)}}$ has been out of date as both $G_8^{(3)}$ and $G_4^{(2)}$ have been updated. Since $G_4^{(2)}$ has just been updated, the messages $m_{G_2^{(1)} \rightarrow G_4^{(2)}}$ and $m_{G_8^{(3)} \rightarrow G_4^{(2)}}$ are up to date and $m_{G_4^{(2)} \rightarrow G_7^{(3)}}$ can be re-computed from tensor contractions of $m_{G_2^{(1)} \rightarrow G_4^{(2)}}$, $m_{G_8^{(3)} \rightarrow G_4^{(2)}}$ and $G_4^{(2)}$. One then updates $G_7^{(3)}$ using the updated messages to it.

One continues the process and sequentially updates $m_{G_7^{(3)} \rightarrow G_4^{(2)}}$ and $m_{G_4^{(2)} \rightarrow G_2^{(1)}}$. One sees that the messages to $G_2^{(1)}$ are up to date, and one updates $G_2^{(1)}$ and then moves on to update all descendants of $G_2^{(1)}$ which are on the branch of $G_3^{(2)}$. One can then update $G_1^{(0)}$ and similarly update all descendants of $G_1^{(0)}$ on the branch of $G_1^{(1)}$, which then finishes the full update of nodes.

To realize the depth-first-search-inspired schedule, all messages need to be initialized. We note that the cost of obtaining all messages is also $O(d)$, and the total complexity of the algorithm is

thus $O(d)$. The approach of initializing all the messages comprised of two steps, whereby the first step is a leaf-to-root sweep computing all messages from a node to its parent, and the second step is a root-to-leaf sweep computing all messages from a node to its children. Figure 13 illustrates our approach to initialize the messages. By sequential tensor contraction, in the leaf-to-root sweep, a node's message to its parent is computed using the messages from the node's children. In the root-to-leaf sweep schedule, one likewise uses sequential tensor contraction to compute the messages from a node to its children, which then allows one to compute the message from the children nodes to their own children nodes.

Algorithm A.1 Alternating minimization.

Require: Training data $\{x^{(i)}, y^{(i)}\}_{i=1}^N$.

Require: Chosen function basis $\{\psi_{i;j}\}_{i=1}^n$ for each $j \in [d]$.

Require: Regularization parameter μ .

Require: Number of iterations R .

- 1: Gather all messages from tensor contractions using the two-step paths exemplified in Figure 13.
- 2: **for** iteration from 1 to R **do**
- 3: **for** each node $q \in Q$ in the depth-first-search path exemplified in Figure 12 **do**
- 4: Update G_q using Equation (A.7).
- 5: Update messages for the next node in sequence using a one-step tensor contraction.
- 6: **end for**
- 7: **end for**

Algorithm summary. The algorithm is summarized as Algorithm A.1, demonstrating the complete procedure for carrying out the alternating minimization algorithm for a given functional hierarchical tensor.

Appendix B. Implementation details of FHT black-box interpolation.

We shall go over how to use the black-box interpolation method to obtain a functional hierarchical tensor representation of function $g(x)$ with access to querying its value at any given point x . For this subroutine, the input is a function g one has access to through evaluation, and the output is the FHT tensor representation of the function g . We note that a similar idea has been explored in the tensor train setting [41, 32].

The algorithm uses the assumption that $g(x)$ has a low-rank structure along a hierarchical bipartition, and it admits a functional hierarchical tensor representation (see Sec. 2 in Ref. [45] for details). For the reader's convenience, important equations in this section are included in Figure 14 in terms of the tensor diagram. Below, we discuss the main equation behind hierarchical black-box interpolation in the functional case.

Equations. We use the notations of the tensor diagram as shown in Fig. 3 for the functional hierarchical tensor. Again, we use C to denote the tensor formed by the contraction of all tensor cores, which satisfies

$$(B.1) \quad g(x) \equiv g(x_1, \dots, x_d) = \left\langle C, \bigotimes_{j=1}^d \vec{\Psi}_j(x_j) \right\rangle.$$

Here, we use similar notations to those defined in Equation (3.1). The symbol G_q denotes a single tensor core, where q is the node of the k -th block at level l . For simplicity, we assume the general case $0 < l < L$ so that q is neither the root nor the leaf node. We define $a := I_{2k-1}^{(l+1)}, b := I_{2k}^{(l+1)}$ and $f = [d] - a \cup b$, where $I_k^{(l)}$ follows notations introduced in Equation (3.2). The structural low-rankness property of FHT implies that there exist $r_a, r_b, r_f \in \mathbb{N}$, $C_a: [n^{|a|}] \times [r_a] \rightarrow \mathbb{R}$, $C_b: [n^{|b|}] \times [r_b] \rightarrow \mathbb{R}$, $C_f: [r_f] \times [n^{|f|}] \rightarrow \mathbb{R}$ such that the following equations hold (illustrated in Figure 14(a)):

$$(B.2) \quad C(i_a, i_b, i_f) = \sum_{\alpha, \beta, \theta} C_a(i_a, \alpha) C_b(i_b, \beta) G_q(\alpha, \beta, \theta) C_f(\theta, i_f).$$

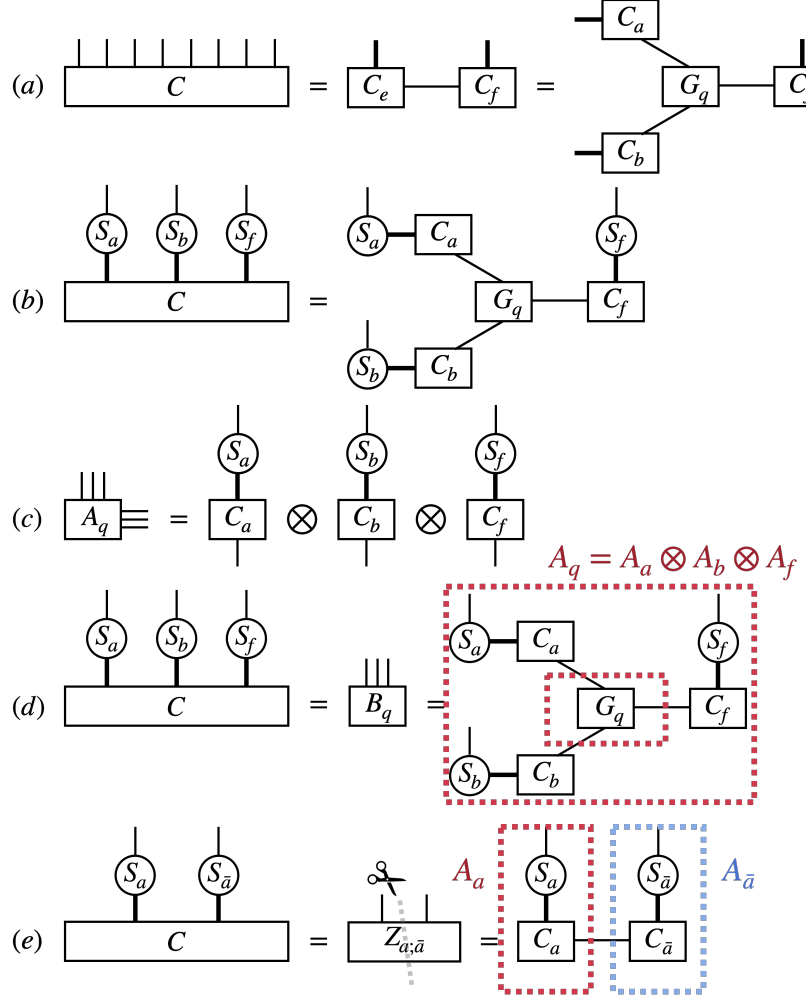


FIG. 14. *Tensor diagram representation of main equations used in Appendix B. Equation (B.2) is summarized in (a). Equation (B.5) is shown in (b). The coefficient term in Equation (B.5) is shown in (c). The definition of B_q is shown in (d). Equation (B.6) for $Z_{\bar{a};\bar{a}}$ is shown in (e), where the scissor symbol indicates the rank- r_a compression through SVD.*

Equation (B.2) is exponential-sized, and one could not solve this equation directly. The hierarchical sketching algorithm [45] introduces sketch functions to solve this over-determined linear system. In this algorithm, we sample structured random points and the evaluation of g on these points derives a sketched version of Equation (B.2), which is the hierarchical sketching algorithm with a specific choice of sketch functions used in [45].

Let $\tilde{r}_a, \tilde{r}_b, \tilde{r}_f$ be integers so that $\tilde{r}_a > r_a, \tilde{r}_b > r_b, \tilde{r}_f > r_f$. To sketch out the exponential-sized tensors C_a, C_b, C_f , we respectively select points $\{x_\mu\}_{\mu \in [\tilde{r}_a]} \subset [-1, 1]^{|a|}$, $\{x_\nu\}_{\nu \in [\tilde{r}_b]} \subset [-1, 1]^{|b|}$, $\{x_\zeta\}_{\zeta \in [\tilde{r}_f]} \subset [-1, 1]^{|f|}$. The evaluation of g on the collected points leads to the following equation

$$(B.3) \quad \forall \mu, \nu, \zeta, \quad g(x^\mu, x^\nu, x^\zeta) = \left\langle C, \bigotimes_{j \in a} \vec{\Psi}_j(x_j^\mu) \bigotimes_{j \in b} \vec{\Psi}_j(x_j^\nu) \bigotimes_{j \in f} \vec{\Psi}_j(x_j^\zeta) \right\rangle.$$

To construct the linear system for G_q , we first use the points (x^μ, x^ν, x^ζ) to construct the right hand side term B_q of the linear system. In this case, the term B_q is obtained by repeated

evaluation of g and given by the following equation:

$$B_q(\mu, \nu, \zeta) := g(x^\mu, x^\nu, x^\zeta).$$

We relate B_q to a sketched-down version of the exponential-sized Equation (B.2). We introduce sketch tensors $S_a: [n^{|a|}] \times [\tilde{r}_a] \rightarrow \mathbb{R}$, $S_b: [n^{|b|}] \times [\tilde{r}_b] \rightarrow \mathbb{R}$, $S_f: [n^{|f|}] \times [\tilde{r}_f] \rightarrow \mathbb{R}$ defined by

$$(B.4) \quad S_a(:, \mu) = \bigotimes_{j \in a} \vec{\Psi}_j(x_j^\mu), \quad S_b(:, \nu) = \bigotimes_{j \in b} \vec{\Psi}_j(x_j^\nu), \quad S_f(:, \zeta) = \bigotimes_{j \in f} \vec{\Psi}_j(x_j^\zeta),$$

and one can readily see that B_q is obtained by contracting the C term in Equation (B.2) with $S_a \otimes S_b \otimes S_f$.

Similarly, the left-hand-side of the linear system for G_q is naturally obtained by the contraction of C_a, C_b, C_f in Equation (B.2) with S_a, S_b, S_f , which leads to the following equation:

$$(B.5) \quad B_q(\mu, \nu, \zeta) = \sum_{\alpha, \beta, \theta} A_a(\mu, \alpha) A_b(\nu, \beta) A_f(\zeta, \theta) G_q(\alpha, \beta, \theta),$$

which is illustrated in Figure 14(b) and Figure 14(d). This linear system is thus

$$(A_a \otimes A_b \otimes A_f) G_q = B_q.$$

The value of A_a, A_b, A_f depends on the gauge degree of freedom in C_a, C_b, C_f , and the detailed procedure of systematically fixing the gauge is introduced in [35, 45]. Here, we briefly explain the procedure. Essentially, we show that one can obtain A_a without having access to C_a . For $\bar{a} := [d] - a$, the structural low-rankness of g implies the existence of $C_{\bar{a}}$ such that there exists a linear system $C(i_1, \dots, i_d) = \sum_{\alpha} C_a(i_a, \alpha) C_{\bar{a}}(\alpha, i_{\bar{a}})$. One can likewise obtain a sketched-down linear system by repeated evaluation of g .

Let $\tilde{r}_{\bar{a}}$ be an integer such that $\tilde{r}_{\bar{a}} > r_a$. Denoting $\mu, \phi \in [\tilde{r}_a], [\tilde{r}_{\bar{a}}]$, we likewise define sketch points as (x^μ, x^ϕ) and sketch tensor $S_{\bar{a}}: [n^{|a|}] \times [\tilde{r}_a] \rightarrow \mathbb{R}$ as $S_{\bar{a}}(:, \phi) = \bigotimes_{j \notin a} \vec{\Psi}_j(x_j^\phi)$. The function g evaluated at the collection of points is given by

$$(B.6) \quad Z_{a; \bar{a}}(\mu, \phi) := g(x^\mu, x^\phi),$$

and subsequently one has (illustrated in Figure 14(e))

$$Z_{a; \bar{a}}(\mu, \phi) = \sum_{\alpha} A_a(\mu, \alpha) A_{\bar{a}}(\alpha, \phi)$$

where $A_{\bar{a}}$ is the contraction of $C_{\bar{a}}$ with $S_{\bar{a}}$. Then, due to a gauge degree of freedom in choosing C_a , there also exists a gauge degree of freedom in choosing A_a . Thus, one can perform singular value decomposition (SVD) on $Z_{a; \bar{a}}$, obtaining $Z_{a; \bar{a}}(\mu, \phi) = \sum_{\alpha} U(\mu, \alpha) V(\alpha, \phi)$, and the choice of $A_a = U$ and $A_{\bar{a}} = V$ forms a consistent choice of gauge between the pair $(C_a, C_{\bar{a}})$.

Likewise, one can obtain $Z_{b; \bar{b}}$ and the SVD of $Z_{b; \bar{b}}$ results in A_b and $A_{\bar{b}}$. The same holds for $Z_{f; \bar{f}}$, A_f , and $A_{\bar{f}}$. To solve for G_q in the linear system Equation (B.5), one simply contracts B_q with the pseudo-inverse of A_a, A_b, A_f . Thus, one can use Equation (B.5) to solve for G_q for any $l \neq 0, L$.

Our construction likewise gives rise to the equation of G_q for $l = 0, L$ as special cases. For $l = 0$, one can go through with the same calculation by setting $C_f = S_f = A_f = 1$ in Equation (B.2) and Equation (B.5). For $l = L$, one can sketch the linear system in Equation (B.2) for $f = [d] - \{k\}$ by contraction with S_f . The details for both cases are described in Algorithm B.1.

Algorithm summary. The algorithm is summarized as Algorithm B.1, which demonstrates the whole procedure to carry out the functional hierarchical tensor sketching algorithm given a sample collection, including the details for the omitted special cases of $l = 0, L$.

Appendix C. Implementation details of FHT-based density estimation.

Algorithm B.1 Functional hierarchical tensor interpolation.

Require: Function $g(x)$.
Require: Chosen function basis $\{\psi_i\}_{i=1}^n$.
Require: Random points $\{x_{I_k^{(l)}}\}, \{x_{[d]-I_k^{(l)}}\}$ generated from $\text{Unif}([-1, 1])$ and target internal ranks $\{r_{I_k^{(l)}}\}$ for each level index l and block index k .

- 1: **for** each node q on the hierarchical tree **do**
- 2: Set l as the level index of q . Set k as the block index of q .
- 3: **if** q is not leaf node **then**
- 4: $(a, b) \leftarrow (I_{2k-1}^{(l+1)}, I_{2k}^{(l+1)})$
- 5: Obtain $Z_{a; \bar{a}}, Z_{b; \bar{b}}$ by Equation (B.6)
- 6: Obtain A_a as the left factor of the best rank r_a factorization of $Z_{a; \bar{a}}$
- 7: Obtain A_b as the left factor of the best rank r_b factorization of $Z_{b; \bar{b}}$.
- 8: **end if**
- 9: **if** q is not root node **then**
- 10: $f \leftarrow [d] - I_k^{(l)}$
- 11: Obtain $Z_{\bar{f}; f}$ by Equation (B.6).
- 12: Obtain A_f as the right factor of the best rank r_f factorization of $Z_{\bar{f}; f}$.
- 13: **end if**
- 14: **if** q is root node **then**
- 15: Obtain $B_q(\mu, \nu) = g(x_a^\mu, x_b^\nu)$.
- 16: Obtain G_q by solving the over-determined linear system $(A_a \otimes A_b)G_q = B_q$.
- 17: **else if** q is leaf node **then**
- 18: Obtain $B_q(\mu, \zeta) = g(x_a^\mu, x_f^\zeta)$
- 19: Obtain Ψ_a as the function values of $\{\psi_i\}_{i=1}^n$ at $\{x_a\}$.
- 20: Obtain G_q by solving the over-determined linear system $(A_f \otimes \Psi_a)G_q = B_q$.
- 21: **else**
- 22: Obtain $B_q(\mu, \nu, \zeta) = g(x_a^\mu, x_b^\nu, x_f^\zeta)$
- 23: Obtain G_q by solving the over-determined linear system $(A_a \otimes A_b \otimes A_f)G_q = B_q$.
- 24: **end if**
- 25: **end for**

In this section, we describe the implementation details of computing an approximate joint density (Markov operator) $P(x, y, o) = \mathbb{P}[X = x, X' = y, O = o]$ using FHT-based density estimation, where we note that in this section, the symbols O, o denote the random variable for the action variable to avoid confusion. We remark that the sketching mechanism in this section relies on sample moment estimation, whereas the sketching mechanism in Appendix B relies on function evaluation. The input to this routine is samples of (X, X', O) , and the output is the joint density P .

We use the interlacing scheme to place the spatial variables on the leaf nodes. We link o to the root node by an extra physical index such that the full tensor diagram represents the functional hierarchical tensor of g . A schematic diagram is shown in Figure 4. We denote the joint variable by $z = (z_1, z_2, \dots, z_{2d}, z_{2d+1}) = (x_1, y_1, \dots, x_d, y_d, o)$.

As the construction for the variable hierarchical bipartition structure and the basis are fixed, one can apply the functional hierarchical tensor sketching algorithm to obtain an FHT-based characterization of the joint density function for $Z = (X, X', O)$. The derivation of hierarchical sketching with the introduction of an action variable does not significantly change the main routine of hierarchical sketching presented in Ref. [45]. Mainly, one needs to modify the relevant sketch functions to take account of the action variable o .

Equations. In the FHT function class, the Markov operator P admits a representation

$$(C.1) \quad P(z) \equiv P(z_1, \dots, z_{2d+1}) = \left\langle C, \bigotimes_{j=1}^{2d+1} \vec{\Psi}_j(z_j) \right\rangle,$$

where $\vec{\Psi}_j$ is the collection of basis functions defined in Equation (3.1) and C is the coefficient tensor. The evaluation of g on the collected points $\{z^{(i)}\}_{i=1}^N$ reads $P(z^{(i)}) = \left\langle C, \bigotimes_{j=1}^{2d+1} \vec{\Psi}_j(z_j^{(i)}) \right\rangle$.

We use G_q to denote a single tensor component, where q is the node of the k -th block at level l . For simplicity, we assume the general case $0 < l < L$ so that q is neither the root nor the leaf node. We define $a := I_{2k-1}^{(l+1)}, b := I_{2k}^{(l+1)}$ and $f = [2d+1] - a \cup b$, where $I_k^{(l)}$ follows notations introduced in Equation (3.2). The structural low-rankness property of FHT implies that there exist $r_a, r_b, r_f \in \mathbb{N}$, $C_a: [n^{|a|}] \times [r_a] \rightarrow \mathbb{R}$, $C_b: [n^{|b|}] \times [r_b] \rightarrow \mathbb{R}$, $C_f: [r_f] \times [n^{|f|}] \rightarrow \mathbb{R}$ such that the following equations hold:

$$(C.2) \quad C(i_a, i_b, i_f) = \sum_{\alpha, \beta, \theta} C_a(i_a, \alpha) C_b(i_b, \beta) G_q(\alpha, \beta, \theta) C_f(\theta, i_f).$$

The hierarchical sketching algorithm essentially solves the over-determined linear system Equation (C.2) for G_q with the use of sketch functions. Let $\tilde{r}_a, \tilde{r}_b, \tilde{r}_f$ be integers so that $\tilde{r}_a > r_a, \tilde{r}_b > r_b, \tilde{r}_f > r_f$. Through the sketch functions $S_a: [n^{|a|}] \times [\tilde{r}_a] \rightarrow \mathbb{R}$, $S_b: [n^{|b|}] \times [\tilde{r}_b] \rightarrow \mathbb{R}$, $S_f: [n^{|f|}] \times [\tilde{r}_f] \rightarrow \mathbb{R}$, one can contract the linear system in Equation (C.2) with S_a, S_b, S_f at the variables i_a, i_b, i_f respectively, which leads to the following sketched linear system:

$$(C.3) \quad B_q(\mu, \nu, \zeta) = \sum_{\alpha, \beta, \theta} A_a(\mu, \alpha) A_b(\nu, \beta) A_f(\zeta, \theta) G_q(\alpha, \beta, \theta),$$

where A_a, A_b, A_f are respectively the contraction of C_a, C_b, C_f by S_a, S_b, S_f and B_q is the contraction of C by $S_a \otimes S_b \otimes S_f$. The sketched-down linear system is thus:

$$(A_a \otimes A_b \otimes A_f) G_q = B_q.$$

We define $s_a: \mathbb{R}^{|a|} \times [\tilde{r}_a] \rightarrow \mathbb{R}$ by

$$s_a(z_a, \mu) = \sum_{i_j, j \in a} S_a(i_a, \mu) \prod_{j \in a} \psi_{i_j}(z_j),$$

and similar one defines s_b and s_f from S_b and S_f . From the definition of s_a, s_b, s_f , the term B_q satisfies

$$B_q(\mu, \nu, \zeta) = \int_{[-1, 1]^{2d+1}} P(z_1, \dots, z_{2d+1}) s_a(z_a, \mu) s_b(z_b, \nu) s_f(z_f, \zeta) dz_1 \dots z_{2d+1},$$

and one has

$$B_q(\mu, \nu, \zeta) = \mathbb{E}_{Z \sim P} [s_a(Z_a, \mu) s_b(Z_b, \nu) s_f(Z_f, \zeta)].$$

As one only has access to samples of the probability density given by P , one uses the approximation of P through empirical distribution, i.e. $P \approx \frac{1}{N} \sum_{i=1}^N \delta_{z^{(i)}}$. Correspondingly, one obtains B_q through finite-sample moment estimation via the equation

$$B_q(\mu, \nu, \zeta) = \frac{1}{N} \sum_{i=1}^N s_a(z_a^{(i)}, \mu) s_b(z_b^{(i)}, \nu) s_f(z_f^{(i)}, \zeta).$$

To compute A_a, A_b, A_f , the work in [45] shows that one similarly needs to compute quantities

$$(C.4) \quad Z_{a; \bar{a}}(\mu, \phi) \approx \frac{1}{N} \sum_{i=1}^N s_a(z_a^{(i)}, \mu) s_{\bar{a}}(z_{\bar{a}}^{(i)}, \phi),$$

obtain $Z_{a; \bar{a}}(\mu, \phi) = \sum_{\alpha} U(\mu, \alpha) V(\alpha, \phi)$ from a singular value decomposition, and take $(A_a, A_{\bar{a}}) = (U, V)$. The procedure also applies to the action-dependent case here. To solve for G_q in the linear system Equation (C.3), one simply contracts B_q with the pseudo-inverse of A_a, A_b, A_f . Thus, one can use Equation (C.3) to solve for G_q for any $l \neq 0, L$.

Our construction likewise gives rise to the equation of G_q for $l = 0, L$ as special cases. For $l = 0$, one can go through with the same calculation by setting $C_f = S_f = A_f = 1$ in Equation (C.2) and Equation (C.3). For $l = L$, one can sketch the linear system in Equation (C.2) for $f = [2d+1] - \{k\}$ by contraction with S_f . The details for both cases are described in Algorithm C.1.

Algorithm summary. The algorithm is summarized as Algorithm C.1, which demonstrates the whole procedure to carry out the action-dependent operator-valued functional hierarchical tensor sketching algorithm given a sample collection.

Algorithm C.1 Action-dependent operator-valued functional hierarchical tensor sketching.

Require: Sample $\{z^{(i)}\}_{i=1}^N$.

Require: Chosen function basis $\{\psi_{i;j}\}_{i=1}^n$ for each $j \in [2d+1]$.

Require: Collection of sketch functions $\{s_{I_k^{(l)}}\}, \{s_{[2d]-I_k^{(l)}}\}$ and target internal ranks $\{r_{I_k^{(l)}}\}$ for each level index l and block index k .

```

1: for each node  $q$  on the hierarchical tree do
2:   Set  $l$  as the level index of  $q$ . Set  $k$  as the block index of  $q$ .
3:   if  $q$  is not leaf node then
4:      $(a, b) \leftarrow (I_{2k-1}^{(l+1)}, I_{2k}^{(l+1)})$ 
5:     Obtain  $Z_{a;\bar{a}}, Z_{b;\bar{b}}$  by Equation (C.4)
6:     Obtain  $A_a$  as the left factor of the best rank  $r_a$  factorization of  $Z_{a;\bar{a}}$ 
7:     Obtain  $A_b$  as the left factor of the best rank  $r_b$  factorization of  $Z_{b;\bar{b}}$ .
8:   end if
9:   if  $q$  is not root node then
10:     $f \leftarrow [2d+1] - I_k^{(l)}$ 
11:    Obtain  $Z_{\bar{f};f}$  by Equation (C.4).
12:    Obtain  $A_f$  as the right factor of the best rank  $r_f$  factorization of  $Z_{\bar{f};f}$ .
13:  end if
14:  if  $q$  is root node then
15:    Obtain  $B_q(\mu, \nu, m) = \frac{1}{N} \sum_i s_a(z_a^{(i)}, \mu) s_b(z_b^{(i)}, \nu) \psi_{2d+1;m}(z_{2d+1}^{(i)})$ .
16:    Obtain  $G_q$  by solving the over-determined linear system  $(A_a \otimes A_b)G_q = B_q$ .
17:  else if  $q$  is leaf node then
18:    Obtain  $B_q(j, \zeta) = \frac{1}{N} \sum_i \psi_{k;j}(z_k^{(i)}) s_f(z_f^{(i)}, \zeta)$ .
19:    Obtain  $G_q$  by solving the over-determined linear system  $(A_f)G_q = B_q$ .
20:  else
21:    Obtain  $B_q(\mu, \nu, \zeta) = \frac{1}{N} \sum_i s_a(z_a^{(i)}, \mu) s_b(z_b^{(i)}, \nu) s_f(z_f^{(i)}, \zeta)$ .
22:    Obtain  $G_q$  by solving the over-determined linear system  $(A_a \otimes A_b \otimes A_f)G_q = B_q$ .
23:  end if
24: end for

```
